QATAR UNIVERSITY

COLLEGE OF ARTS AND SCIENCES

IMPACT OF PROLONGED EXPOSURE TO SOUR SERVICE ON THE MECHANICAL PROPERTIES AND CORROSION MECHANISM OF NACE CARBON STEEL MATERIAL USED IN WET SOUR GAS MULTIPHASE PIPELINE IN QATAR

BY

MANOJ YADAV

A Thesis Submitted to

the College of Arts and Sciences

in Partial Fulfillment of the Requirements for the Degree of

Masters of Science in Material Science and Technology

June 2020

COMMITTEE PAGE

The members of the Committee approve the Thesis of
Manoj Yadav defended on 11/05/2020.

_____
Dr. Aboubakr M. Abdullah
Thesis/Dissertation Supervisor

_____
Dr. Khaled Youssef
Committee Member

_____
Dr. Abdul Shakoor
Committee Member

Approved:

_____
Ibrahim AlKaabi, Dean, College of Arts and Sciences

ABSTRACT

YADAV MANOJ , Masters : June : [2020], Material Science and Technology

Title: Impact of Prolonged Exposure to Sour Service on the Mechanical Properties and Corrosion Mechanism of NACE Carbon Steel Material Used in Wet Sour Gas Multiphase Pipeline in Qatar.

Supervisor of Thesis: Dr. Aboubakr M. Abdullah

Oil and Gas industries involve severe corrosive/sour environmental conditions due to H_2S and CO_2 and moisture content. The National Association of Corrosion Engineers, NACE, has developed standards to enable the users to select suitable material for given sour conditions by means of laboratory testing. This thesis takes up the study of a failed (corroded) piping sample (API-5L-X65) removed from a pipeline after 15 years of service. Mechanical properties of the removed samples (both corroded as well as non-corroded) were evaluated and compared. Pitted samples were analyzed using a scanning electron microscope coupled with energy dispersive X-ray (SEM/EDS) for understanding the morphology of the deposits. EDS results were further compared using XPS analysis. Optical microscopy was used to compare the microstructure of the corroded sample near the surface exposed to the service environment and away from it. Micro-hardness was carried out on the cross-section of the removed sample to understand any evident hardness variation from ID to OD of the piping. The electrochemical behavior using Electrochemical Impedance Testing (EIS) of the corroded sample (with corrosion scales) was tested in 5% sodium sulfate solution, and the results were compared with the un-corroded part (polished) of the same sample. All the results suggest that prolonged service exposure has resulted in the development of micro defects, resulting in the reduction of strength and impact toughness along with the reduction in the hardness at the exposed surface of the corroded piping. Understanding the material behavior due to long-term exposure will surely help

the industry in repair/replacement planning while extending the usable design life of the material. The results acheived during this thesis, will surely pave the way for oil & gas industry to develop further ways to monitor the changes in the critical material properties when exposed to sour services.

DEDICATION

This thesis is dedicated to my parents, my wife, and my children- Gargee and Viplav for their continuous motivation, support, and unconditional love.

ACKNOWLEDGMENTS

I would like to express my sincere gratitude to my supervisor, Dr. Aboubakr M. Abdullah, for his constant guidance, encouragement, and support throughout my graduate studies program.

Many thanks go to Dr. Khaled Youssef, who gave me much needed support, guidance, and many helpful suggestions during my thesis.

I would also like to thank Mr. Ahmed Soliman and Mr. Mostafa Sliem, who helped me to carry out various experimental parts of my thesis.

A big thank goes to Mr. Ibrahim Ali Muzghi, who inspired me to carry out this study and also authorized me to use the corroded pipe spools, for carrying out the subject study.

TABLE OF CONTENTS

LIST OF TABLES

LIST OF FIGURES

CHAPTER 1: INTRODUCTION

Handling of wet hydrogen sulfide (H_2S) is one of the major challenges in the oil and gas industry. H_2S is a threat to equipment/piping reliability, along with being a life-threatening gas. Two modes of failures are associated with wet H_2S: cracking and thinning (localized/general). Several industrial standards have been developed for design, material selection, and fabrication of equipment handling wet H_2S service. However still, failures related to sour service are common in the oil and gas industry. Wet H_2S has a major effect on steel as it charges it with nascent hydrogen and thus influencing its significant mechanical properties like tensile strength, ductility, and fracture toughness [1]. This change in critical mechanical properties can affect the functioning of material during operation and may lead to failures. More so, feed gas coming from wellheads carries H_2S, CO_2, chlorides, and organic acids that can cause accelerated corrosion/thinning in carbon steel pipes. Factors affecting corrosion rates are flow, temperature, pressure, dead legs, gas composition, corrosion inhibitor (CI) performance, etc. To add more complexity, other chemicals, like hydrate inhibitors, are also injected in the feed gas, to prevent hydrates formation during winter seasons. However, many efforts are made in simulating the field conditions while selecting corrosion and hydrate inhibitors, but it is always difficult to create actual field environment due to huge amount of variables. Hence, under current research project, scope is to study actual piping component, which has been in sour feed gas service for around 15 Years and have shown significant corrosion. The corrosion deposits observed on the pitted samples were studied by scanning electron microscope (SEM) imaging and X-ray photoelectron spectroscopy (XPS) analysis. Electrochemical impedance spectroscopy measurements were also done on the corroded samples to understand the

performance/property of the corrosion scales. The research sample was a part of the 2” piping spool, which is associated with a slug catcher inlet pipeline of a gas plant situated in the State of Qatar. An actual piping sample, which has been exposed for 15 years in sour service in the wet gas multiphase pipeline, was tested for its mechanical properties. The selected 2” piping spool had seen active corrosion and was replaced based on the severe localized thickness loss. Current research indicates that hydrogen charging impacts the critical mechanical properties of the material [1-3]. The impact was quantified for actual in-service piping material under a specific sour service environment. This information will be utilized for developing future maintenance philosophy for the complete pipeline, based on the severity of the observed impact. In addition, this information will be used for developing repair plans during the replacement of corroded sections of a slug catcher and its associated piping. Following major properties was measured for the exposed sample and it was compared with the new material of the same specification:

a) Tensile strength

b) Yield strength

c) Ductility

d) Impact properties

e) Micro Hardness

CHAPTER 2: LITERATURE REVIEW

2.1. Current Understanding On Damage Mechanism Associated With Sour Service:

Researchers and engineers have understood the criticality of handling wet H_2S containing fluids as it can cause catastrophic failures of pressure parts, releasing poisonous and flammable gas in the environment. Such failures are a threat to people as well as to a plant. Damage mechanisms associated with sour service are well established and explained in international codes and standards. Wall thinning (localized/general) and cracking are two modes of failures associated with sour service environments.

2.1.1. Cracking damage mechanisms:

Following paragraph briefly describes the primary damage mechanisms with cracking failure mode, associated with sour service:

a) **Sulfide Stress Cracking (SSC):** Cracking of a metal under the combined action of tensile stress and corrosion in the presence of water and H_2S. SSC usually occurs more readily in high strength steels or hard weld zones of steel.

b) **Hydrogen Blistering:** It is a phenomenon of formation of subsurface cavities, called hydrogen blisters, in a metal resulting from excessive hydrogen pressure. Hydrogen blistering in steel involves the absorption and diffusion of atomic hydrogen produced on the metal surface by the sulfide corrosion process. The absorbed atomic hydrogen sits in the internal trap sites (like-nonmetallic inclusions, laminations, or other discontinuities) and recombined to form molecular hydrogen gas, which is too large to diffuse through steel.

c) **Hydrogen Induced Cracking (HIC):** It is stepwise internal cracks that connect adjacent hydrogen blisters on different planes in the metal or to the metal surface. No externally applied stress is needed for the formation of HIC. HIC is commonly found in steels with high impurity levels or regions of anomalous microstructure produced by segregation of impurities and alloying elements in the steel [4].

d) **Galvanically Induced Hydrogen Stress Cracking (GIHSC):** GIHSC describes cracking in metals that are not sensitive to SSC but which can be embrittled by hydrogen when galvanically coupled, as the cathode, to another metal that is corroding actively as an anode [5].

2.1.2. Thinning damage mechanisms:

Another mode of failure, which is equally important while selecting and operating in sour service, is wall thinning (Corrosion) associated with sour service (wet gas multiphase pipelines). When carbon steel is exposed to wet sour gas, the initial corrosion rate is very high, which slows down with time due to the formation of iron sulfide scales. A typical plot of corrosion rates versus time [6] using electrochemical techniques is shown in Fig. 1.

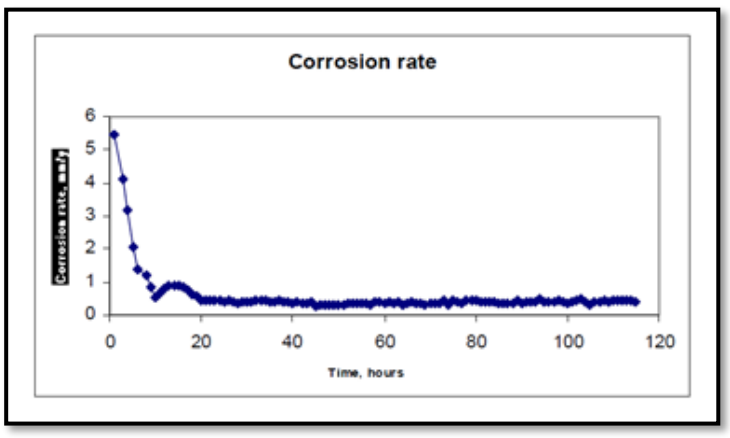

Figure 1. Corrosion rate of carbon steel in sour media [6]

The formation of a uniform adherent Fes layer, which can protect further corrosion seldom, happens in real production scenarios. Thus, corrosion rates of as high as 50mm/year is not uncommon in a wet sour system [7]. The quality of a FeS layer depends upon the following parameters:

1. Type of flow (stratified/slug or wave flow)
2. H_2S and CO_2 partial pressure
3. Water salinity
4. Presence of chlorides, element Sulphur
5. Amount of organic acids in the process
6. Deposition of other solids
7. Presence of dead legs
8. CI performance

Following are major corrosion types associated with wet gas multiphase pipelines:

a) **Top of Line (TOL) Corrosion:** Top of line corrosion happens under stratified flow conditions at 10 to 2'O clock position, when water vapor in the gas is condensed upon the cold surface of the steel. Interaction between mutually condensing liquid hydrocarbon and water is poorly understood and requires further dedicated research. TOL corrosion is generally controlled using corrosion inhibitor (CI) at flow rates high enough to reach the top of the line. Batch inhibitors are used at lower flow rates, to ensure that the complete pipeline surface is passivated with a CI.

b) **Bottom of the Line (BOL) Corrosion:** This term is used for a variety of corrosion reactions happening at the bottom half of the pipeline (between-3 to 9' O clock). Long term corrosion rate of the system depends upon the quality of the FeS layer. When the FeS layer is semi protective or not uniformly formed tendency of pitting in the pipeline increases, in such systems, careful

monitoring of corrosion inhibition system is of utmost importance to avoid pitting initiation. BOL corrosion is also mitigated by using appropriate CI. However, the efficiency of the CI beneath the FeS layer remains a challenge. If a localized pit has formed inside the pipeline, where formed FeS layer is loose and permeable, making it difficult for CI to prevent further corrosion at the base of the pit. Thus prevention of pit initiation is a key priority in sour service pipelines.

c) **Under Deposit Corrosion**: Gas field wells produce a varying quantity of sand along with gas, water, and liquid hydrocarbon. Sand and FeS layer lying at the bottom of the pipe can lead to the under deposit corrosion as the ability of CI to penetrate beneath the deposits is highly variable. Hence, a regular pigging program is necessary to remove deposits from a pipeline to avoid under deposit corrosion.

d) **Dead leg Corrosion**: Effect of quality of FeS layer on corrosion rates have been discussed above. Accelerated corrosion occurs when the FeS layer is removed due to the intermittent wetting of pipelines. This mechanism is more dangerous for small bore piping as they have usually lower thickness. Identification of dead legs and developing of an inspection program is key to avoid failures.

e) **Galvanic Corrosion**: Galvanic corrosion occurs when two dissimilar materials are bolted or welded together in the presence of the conductive and corrosive environment. In the presence of an electrolyte, differences in the electrochemical potential of the metals can drive corrosion into the more electronegative material, which can result in localized corrosion near the metal joint.

f) Effect of Glycol on Corrosion Inhibitor efficiency/Corrosion Rates: During winter seasons, some of the pipelines have to be treated with glycol to prevent

hydrate formation. The glycols are generally considered inert to the electrochemical corrosion, and lots of work has been done to ascertain the positive impact on glycol on corrosion rates in sweet service. However, much is not known on the impact of glycol (how it affects the Fes layer) corrosion rates in pipelines with sour service.

2.2. International Codes and Standards-Importance and Limitations:

International standards have been developed for selecting the material, which is resistant to cracking mechanisms explained above. National Association of Corrosion Engineers (NACE) developed a document-NACE-MR0175/ISO15156- 1/2/3- which provides detailed guidelines for the selection of materials in a various sour environment. This standard addresses all the mechanisms associated with the wet H_2S, e.g., the sulfide-stress corrosion cracking (SSCC), hydrogen-induced cracking (HIC), and galvanically-induced hydrogen stress cracking (GIHIC).

As per NACE standard MR0175/ISO15156, the severity of the sour environment can be identified using the chart, given below in Figure 2. While determining the severity of the wet H_2S containing environment, the worst case scenario needs to be considered, including process upset conditions or shutdown time.

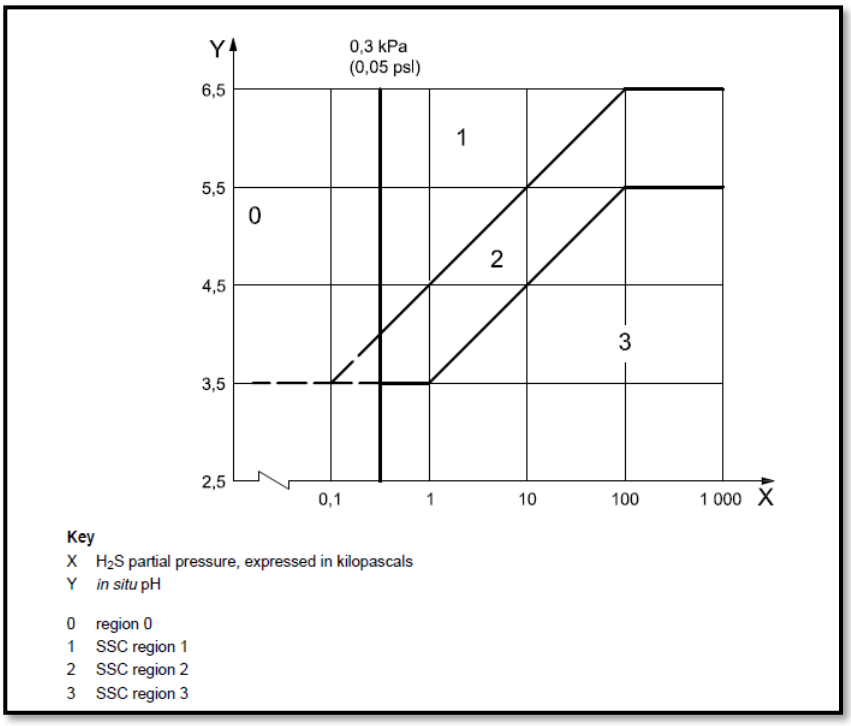

Figure 2. Regions for environmental severity W.R.T SSCC of CS and LAS [6]

The standard provides us guidelines to select the material for each severity region. If the suitable material choice is not available, the standard allows the user to test any material for a specific range of sour conditions. Even if the material is selected from the listed materials provided in the NACE-MR0175/ISO-15156 standards, a user needs laboratory testing for HIC, Stress-oriented hydrogen-induced cracking (SOHIC), and soft-zone cracking (SZC). Standard provides guidance on test methods and acceptance criteria. The laboratory testing tries to replicate field conditions for the very little duration, where the major concern is to choose the parameters for the intended service. It is always impractical to consider all the possibilities of in-service scenarios.

As stated above, nascent hydrogen is generated in sour service environments, which get absorbed in the steel during operations. Most researchers and investigators have indicated that the predominant effect of hydrogen on the properties of steel is a decrease in ductility and true stress at fracture [1]. This may lead to loss of load-carrying capacity, cracking, and

delayed cracking of steels. However, most of the test methods used to reach the above conclusions were made while using fresh metallic samples, which were impregnated by hydrogen using laboratory conditions.

So carrying out testing on a pipe sample which was exposed to sour service (wet gas multiphase pipeline) for 15 years, can provide useful insights on material behavior after actual service exposures, which includes slowdowns, shutdowns, Corrosion inhibitor/ Hydrate inhibitory injections, and operations at various pressures and temperature.

The proposed thesis has focused on the analysis of the mechanical properties of the actual piping sample that has been exposed to sour service for 15 years. Existing literature and research had focused on the fresh samples, which were impregnated with hydrogen in Labs. It is near impossible to simulate every possible scenario in LAB, and thus the lab results may not reflect the correct picture. Hence, the results of this research will provide useful insight into the effect of long-term exposure on the mechanical properties of the material.

Replacement of a section of piping or repairs in equipment is a regular practice for the oil and gas industry. Usually, extensive replacement repairs calls for hydrotesting of a complete piping loop or equipment to prove the mechanical integrity of the repaired system. However, since the hydrotest loop contains both new and old components (which have been exposed to sour service), carrying out hydrotest at design hydrotest pressure (1.5 X Design pressure) may damage the already week/degraded old components. Thus, the results of this part of the research will also help the industry to align on the testing requirements after repair or replacement job in case of sour service.

As explained above, each gas field possesses a unique challenge with respect to corrosion damages in pressure equipment and piping. Understanding individual field-specific corrosion mechanisms is of utmost importance for the reliable and safe operation of sour gas multiphase pipelines.

Current published literature focuses on TOL and BOL corrosion. However, the failed sample, used for the proposed research, showed most of the corrosion at 3' O clock and at 9' O clock position. The proposed research will investigate the reason behind this corrosion. Also, as per the available literature, the effect of glycol on sweet corrosion is well established, but it cannot be said for sour service [8]. The pipeline from which the research sample has taken also used glycol as anti-hydrate during the winter season. The proposed research will investigate the role of glycol in the localized pitting happened in the sample.

All the above research questions should provide some answers to the complex problem of localized corrosion happening in the wet sour gas multiphase pipeline and will help to fill the existing gaps and thus to achieve better corrosion management.

2.3. Summary of Similar Work Done in Past:

Lots of work has been done in the past, for evaluating the effect of hydrogen charging in the steels. In one such experiment, API-5L X65 (In-service) piping was used to understand the effect of hydrogen charging on its mechanical properties. However, the service of this piping was non-sour, and non-corroded samples were used for experiments. Hydrogen was charged in the specimen while carrying out mechanical testing. Hydrogen was generated in the steel due to its reaction to the testing solution. Ductility was measured in terms of elongation and reduction in area, and results were compared between hydrogen-charged and normal steels. Significant reduction in ductility at room temperature (both in terms of elongation and reduction in area) was observed in the steel. This proves that the pre-charging of pipeline steels to certain hydrogen contents can cause irreversible changes in the anelastic and mechanical properties of steels and result in modification of the fracture surface and hydrogen permeation process [9].

In another paper, the influence of hydrogen and low temperature on mechanical properties of two pipeline material, X65, and F22 low alloy steel was studied. New material was used in the

experiment, and an electrochemical set up was utilized for hydrogen charging. The diffusable hydrogen content of steels was kept in the range of 0.6 to 2 PPM. The Charpy test was done on both X65 and F22 samples with and without hydrogen charged specimen. A slight reduction in upper shelf energy along with scattered results for both energy and brittle area values was observed for hydrogen charged specimens [10].

From the literature survey, it is evident that not many results about the effect of hydrogen on mechanical properties of ferritic steels are available, and also reported results are not always consistent. For example, a decrease in ductility (elongation/area reduction) was always reported in the presence of hydrogen, but both increase and decrease in the yield strength in the presence of hydrogen have been reported by various authors.

CHAPTER 3: EXPERIMENTAL WORK

3.1. Samples Details:

3.1.1. Location of Sample: The corroded sample, analyzed under this research, was part of a wet gas inlet pipeline coming from offshore and going to slug catcher. The corroded piping was 2" bypass of an emergency shutdown valve (ESDV13) installed on 38" mainline.

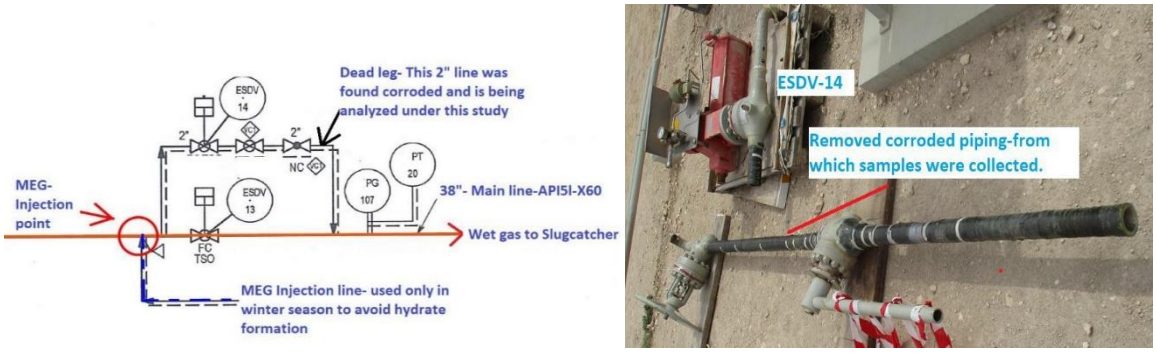

Figure 3. Showing the actual location of corroded sample analyzed under this project

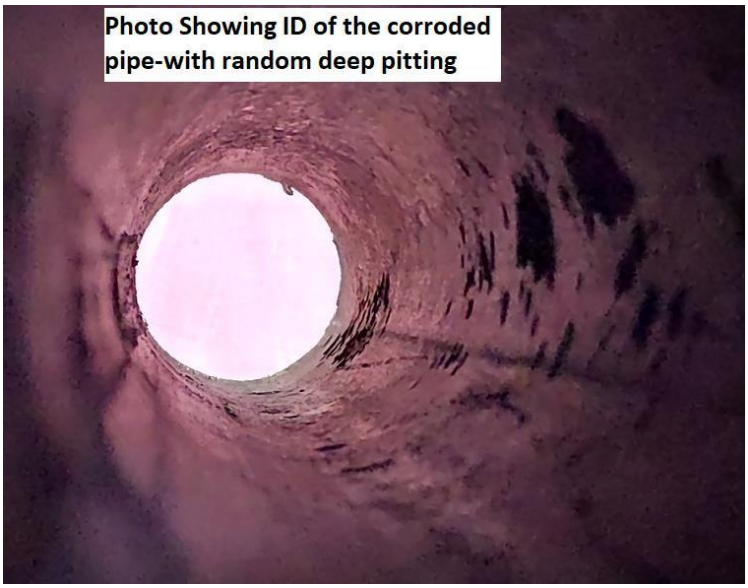

Figure 4. Showing ID of failed spool

3.1.2. Metallurgy of Sample: The corroded piping metallurgy is API5L-X60 (NACE). The nominal thickness of the 2” piping is 8.74 mm. The below tables provide the chemical composition and mechanical properties of the material as per specification.

Steel Grade	Mass Fraction Based on Heat and Product Analyses % max									Carbon Equivalent [a] % max	
	C [b]	Si	Mn [b]	P	S	V	Nb	Ti	Other [c,d]	CE_{IIW}	CE_{Pcm}
SMLS and Welded Pipe											
L390QS or X56QS	0.16	0.45	1.65	0.020	0.003 [e]	0.07	0.05	0.04	[g]	0.40	0.21 [h]
L415QS or X60QS	0.16	0.45	1.65	0.020	0.003 [e]	0.08	0.05	0.04	[g,i,k]	0.41	0.22 [h]
L450QS or X65QS	0.16	0.45	1.65	0.020	0.003 [e]	0.09	0.05	0.06	[g,i,k]	0.42	0.22 [h]

[a] Based on product analysis (see 9.2.4 and 9.2.5). The CE_{IIW} limits apply if C > 0.12 % and the CE_{Pcm} limits apply if C ≤ 0.12 %.

[b] For each reduction of 0.01 % below the specified maximum for C, an increase of 0.05 % above the specified maximum for Mn is permissible, up to a maximum increase of 0.20 %.

[c] Al_{total} ≤ 0.060 %; N ≤ 0.012 %; Al/N ≥ 2:1 (not applicable to titanium-killed or titanium-treated steel); Cu ≤ 0.35 % (if agreed, Cu ≤ 0.10 %); Ni ≤ 0.30 %; Cr ≤ 0.30 %; Mo ≤ 0.15 %; B ≤ 0.0005 %.

[d] For welded pipe where calcium is intentionally added, unless otherwise agreed, Ca/S ≥ 1.5 if S > 0.0015 %; for SMLS and welded pipe, Ca ≤ 0.006 %.

[e] The maximum limit for S may be increased to ≤ 0.008 % for SMLS pipe and, if agreed, to ≤ 0.006 % for welded pipe; for such higher S levels in welded pipe, lower Ca/S ratios may be agreed.

[f] Unless otherwise agreed, Nb + V ≤ 0.06 %.

[g] Nb + V + Ti ≤ 0.15 %.

[h] For SMLS pipe, the listed CE_{Pcm} value may be increased by 0.03.

[i] If agreed, Mo ≤ 0.35 %.

[j] If agreed, Cr ≤ 0.45 %.

[k] If agreed, Cr ≤ 0.45% and Ni ≤ 0.50%.

Figure 5. Chemical composition of a sample as per specification

Pipe Steel Grade	Pipe Body of SMLS and Welded Pipe						Weld Seam of HFW and SAW Pipe
	Yield Strength [a] $R_{t0.5}$ MPa (psi)		Tensile Strength [a] R_m MPa (psi)		Ratio [b] $R_{t0.5}/R_m$	Elongation (on 50 mm or 2 in.) A_f %	Tensile Strength [c] R_m MPa (psi)
	min	max	min	max	max	min	min
L415QS or X60QS L415MS or X60MS	415 (60,200)	565 (81,900)	520 (75,400)	760 (110,200)	0.93	e	520 (75,400)
L450QS or X65QS L450MS or X65MS	450 (65,300)	600 (87,000)	535 (77,600)	760 (110,200)	0.93	e	535 (77,600)
L485QS or X70QS L485MS or X70MS	485 (70,300)	635 (92,100)	570 (82,700)	760 (110,200)	0.93	e	570 (82,700)

[a] For intermediate grades, the difference between the specified maximum yield strength and the specified minimum yield strength shall be as given in the table for the next higher grade, and the difference between the specified minimum tensile strength and the specified minimum yield strength shall be as given in the table for the next higher grade; for intermediate grades, the tensile strength shall be ≤ 760 MPa (110,200 psi).

[b] This limit applies for pipe with $D > 323.9$ mm (12.750 in.).

[c] For intermediate grades, the specified minimum tensile strength for the weld seam shall be the same value as was determined for the pipe body using footnote a).

[d] For pipe requiring longitudinal testing, the maximum yield strength shall be ≤ 495 MPa (71,800 psi).

[e] The specified minimum elongation, A_f, on 50 mm or 2 in., expressed in percent and rounded to the nearest percent, shall be as determined using the following equation:

$$A_f = C\frac{A_{xc}^{0.2}}{U^{0.9}}$$

where

C is 1940 for calculations using SI units and 625,000 for calculations using USC units;

A_{xc} is the applicable tensile test piece cross-sectional area, expressed in square millimeters (square inches) as follows:

1) for circular cross-section test pieces, 130 mm² (0.20 in.²) for 12.7 mm (0.500 in.) and 8.9 mm (0.350 in.) diameter test pieces, and 65 mm² (0.10 in.²) for 6.4 mm (0.250 in.) diameter test pieces;
2) for full-section test pieces, the lesser of a) 485 mm² (0.75 in.²) and b) the cross-sectional area of the test piece, derived using the specified outside diameter and the specified wall thickness of the pipe, rounded to the nearest 10 mm² (0.01 in.²);
3) for strip test pieces, the lesser of a) 485 mm² (0.75 in.²) and b) the cross-sectional area of the test piece, derived using the specified width of the test piece and the specified wall thickness of the pipe, rounded to the nearest 10 mm² (0.01 in.²);

U is the specified minimum tensile strength, expressed in megapascals (pounds per square inch).

Figure 6. The mechanical properties of the sample as per specification.

3.1.3. Operating Conditions: This corroded portion of the piping was a dead leg (Portion of piping with no flow/intermittent flow). However, it was exposed to the operating fluid, which is sour wet gas, which has three phases (vapor, liquid condensate, and water). The operating temperature is around room temperature, and pressure is 80 bar(g). Normal composition of the process fluid is provided in the below table.

STREAM			
V/L STATE	Vapor	Liquid	Water
Composition [mol%]			
H20	0.07	0.06	93.02
H2S	1.94	3.23	0.12
CO2	3.64	2.66	0.08
He	0.05	0.01	0.00
N2	5.20	0.72	0.00
C1	81.29	27.17	0.00
C2	4.65	5.42	0.00
C3	1.70	4.94	0.00
iC4	0.33	1.85	0.00
nC4	0.52	3.78	0.00
iC5	0.17	2.41	0.00
nC5	0.15	2.57	0.00
C6+	0.24	41.90	0.00
Aromatics	0.02	2.69	0.00
Sulfur Compound	0.03	0.59	0.00
MEG	0.00	0.00	6.78
TOTAL FLOW, kg.mol/h	71229	3348	772.9
TOTAL FLOW, kg/h	1419247	253734	16286
MOLECULAR WT	19.9	75.8	21.1
DENSITY, kg/m3	78.1	653.2	1058
VISCOSITY, cP	0.014	0.334	3.40

Figure 7. Chemical composition of the Service fluid

3.1.4. *Visual Inspection findings of the Corroded spools*: Two pipe spools (A- 9 inch & B- 8 inch) were cut from the removed piping for investigation purposes. The bottom (6'0 clock) position was marked in both spools. Please note that the corroded piping was externally composite wrapped to avoid failure during operations. Composite wrapping is visible in the sample photographs. Close visual inspection was carried out on as-removed samples.

Following, are few critical observations made on the collected samples:

a) Both samples showed a band of yellow marking @ 4'O clock position.

b) Random pitting was observed on both the samples.

c) The severity of pitting was maximum at 9-10'O clock position and near the yellow marking.

Figure 8. Micrographs highlighting all critical observations.

3.2. Sample Preparation and Testing:

The above two piping spools were utilized to prepare the testing specimen for Mechanical as well as Corrosion testing.

3.2.1. *Tensile Samples*: Six Standard samples as per ASTM standard E8/E8M-16a were prepared. Three samples were without evident thinning/pitting at the reduced parallel section, whereas the other three samples were prepared with the pitting/corroded area within the reduced parallel sections.

Figure 9. Photograph for the tensile samples (T1-T6).

Ultrasonic thickness meter was utilized to measure the actual minimum thickness of the tensile specimens.

Figure 10. UT measurements for identifying the lowest thickness area in corroded specimens.

The minimum area of the specimen was calculated based on ASTM standard E8/E8M-16a. The following table provides a summary of the thickness and calculated area for each specimen.

Table 1. The minimum calculated area for each tensile sample

Sample No.	Width (mm)	Dia (mm)	Thickness (minimum)	CalculatedArea (mm^2)
T1	12.5	60.3	7.9	100.12
T2	12.5	60.3	7.7	97.26
T3	12.5	60.3	7.9	100.12
T4	12.5	60.3	6.1	76.75
T5	12.5	60.3	6.7	84.38
T6	12.5	60.3	7.4	93.1

3.2.2**.** *Tensile Testing***:** Tensile testing of all the six samples was carried out using the Instron Universal testing machine. Strain rate for sample –T1 was kept as 10^{-4} /Sec, while for rest, the strain rate was kept as 10^{-3}/sec.

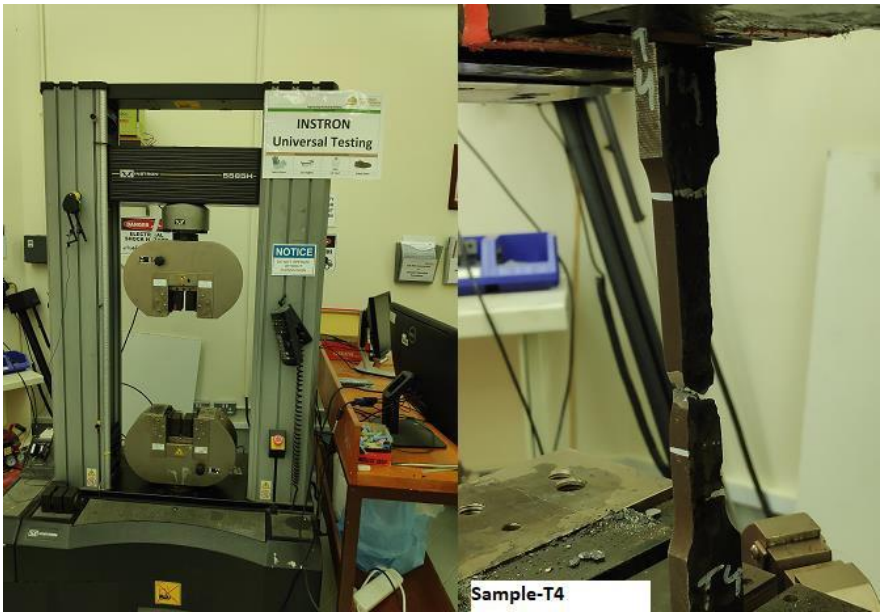

Figure 11. Photograph for the tensile machine and one failed sample

3.2.3. *Impact Samples/Testing*: Five standard samples were prepared as per ASTM standard E23. Three samples were polished and provided with the notch in the center. However, the remaining two samples were prepared without polishing, with the pitted area at the center. Impact testing for all samples was carried out at room temperature by using Avery- Dension, UK –Impact Testing machine.

Figure 12. Photograph for the impact machine and impact samples.

3.2.4. *Corrosion samples*: The following 12 specimens (1 x 1 cm^2) were cut for carrying out corrosion assessment of the spools.

Table 2. Sample details and characterization techniques.

Sample Name	No of specimen	No of specimen	No of the specimen in Blank area (no pits)	Corrosion Testing/Characterization
A (9 inch)	2 (A1/A2)	2 (A3/A4)	2 (A5/A6)	Optical- Corroded sample XPS-All samples SEM/EDS-All samples + Fracture
B (8 inch)	2 (B1/B2)	2(B3/B4)	2(B5/B6)	

The following characterizations were carried out on the above spools:

a) XPS Analysis: Surface composition of all samples was analyzed by X-ray photoelectron spectroscopy (XPS), Model Axis (Ultra DLD XPS Kratos, Manchester, UK), equipped with a monochromatic Al Kα radiation source (1486.6 eV) X-ray Power, 15 kV, 20 mA under a UHV environment (ca. 5x10-9 Torr). XPS is equipped with a set of chambers to transfer sensitive samples from the sample transfer chamber (STC) to the XPS surface analysis chamber (SAC) which is under ultra-high vacuum.

Figure 13. Photograph for the used XPS machine.

b) **SEM/EDS Analysis:** The SEM instrument used in this work was Nova Nano SEM 450, with a voltage capability ranging from 200 V to 30 kV. All the samples (A1-A6 and B1-B6) were scanned without removing corrosion products or deposits. Additionally, the fractured surface of the two tensile samples (T2 and T4) were compared using this technique to understand the difference in the surface morphology of the failed corroded and non-corroded samples. The scanning electron microscope is a class of microscope that uses focused electron beams instead of light; it scans the surface of the sample and produces an image with an extremely high resolution. Electron/sample interaction produces different forms of signals using Secondary Electrons (SE), Backscattered electrons and diffracted back scattered electrons. Secondary Electrons (SE), are most valuable for showing morphology and topography on samples. And Backscatered Electrons are useful for illustrating contrast in composition in multiphase samples[11].

c) **Energy Dispersive X-ray spectroscopy** is an accessory included in most modern SEMs. Its objective entails exciting an inner shell electron from the sample by bombarding it with an electron beam, subsequently causing an electron from a higher energy shell to substitute the previously excited electron emitting an x-ray. Leading to a fingerprint signal formed by the electron traveling between shells, EDX is capable of depicting the results in both spectrum and map form [12].

Figure 14. Photograph for the used SEM machine.

d) **Microhardness & Optical Microscopy:** Two corroded samples were polished, and microhardness was taken across the cross-sectional area to understand the difference in hardness from the inner diameter (ID) to the outer diameter (OD) of the samples. The ID of the sample was exposed to sour service and thus having corroded surface, while as, OD have not directly seen the service fluid. Microhardness is a method of determining a material's hardness or resistance to penetration when test samples are very small/thin [13]. It is used to get precise and detailed information about surface features and its hardness variation. The machine used during testing of samples was FM100. The same samples were utilized to carry out optical microscopy to understand the difference in the microstructure near ID and of the bulk material.

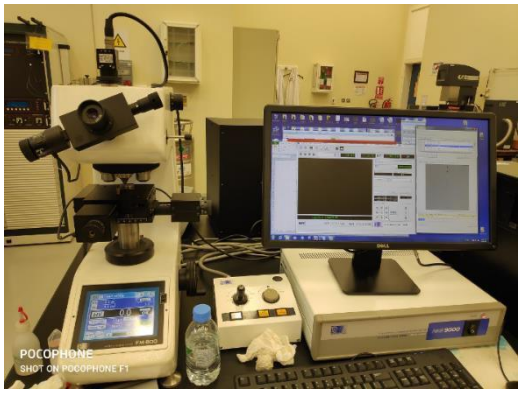

Figure 15. Photograph for the used microhardness machine.

e) Electrochemical Impedance Spectroscopy (EIS): Electrochemical measurements were performed in a three-electrode double-jacketed cell for both corroded and non-corroded samples (polished). Both the samples with an exposed area of 0.5 cm^2 were used as working electrodes, and a graphite rod was used as an auxiliary electrode. An Ag/AgCl electrode was employed as a reference electrode. The reference electrode is coupled with a Luggin capillary to minimize the potential drop between the electrodes. The C-steel was immersed in the test solution for 30 minutes before each electrochemical test to achieve a steady-

state condition. The EIS analyses were performed under an open circuit potential (OCP) condition at a frequency range of 1×10^{-1} to 1×10^{5} Hz, with an AC amplitude of ±10 mV, using a GAMRY 3000 potentiostat (Gamry, Warminster, PA, USA) as seen in Figure 16. To ensure the reproducibility of the measurements, each test was repeated three times.

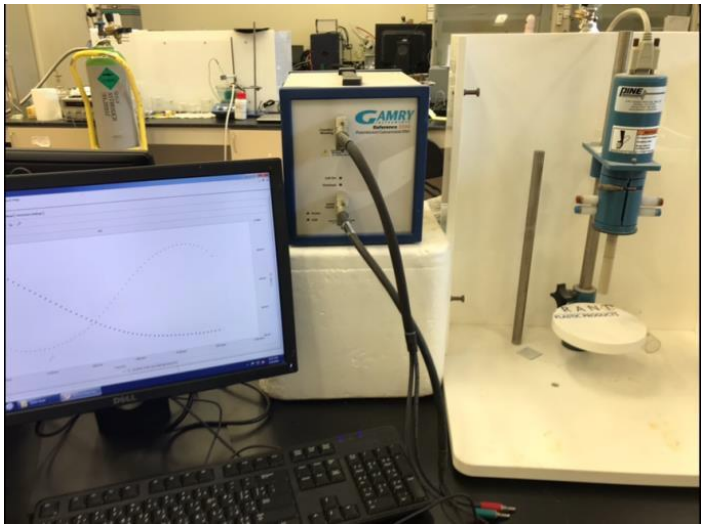

Figure 16. Photograph Showing Impedance testing of corroded and non-corroded samples (Potentiostat instrument, Model: GAMRY "Reference 3000")

CHAPTER 4: RESULTS AND DISCUSSIONS

4.1. Tensile results

The following table provides a summary of results for all tensile samples

Table 3. The measured mechanical properties of the tested samples.

Sample Name	Non-Corroded			Corroded			Standard Values for X60 Steel
	T1* (10^{-4} mm/sec)	T2	T3	T4	T5	T6	
Yield Stress (Mpa)	304.7	298.16	303.4	325.9	326.04	333.16	415-565
UTS (Mpa)	457.9	456.35	465.24	507.77	511.99	497.3	520-760
% elongation	38%	40%	39%	23.60%	29.90%	36%	17.5 % (minimum)

*For Tensile samples (T2-T6) Strain rate used was 10^{-3} mm/sec

Corroded samples were showing higher Yield stress and UTS when comparing to non-corroded samples, however absolute values for both samples were significantly lower than the standard values. This suggests that complete in-service piping has been affected by the long exposure to sour service irrespective of the corrosion condition. However, the effect on the corroded portion seems to be less aggravated in terms of reduction in Yield stress and UTS, but at the expense of % elongation.

The elongation% values were found significantly higher than the standard values. However, the stark difference can be noticed between the corroded and non-corroded samples. Corroded samples exhibited lower values of % elongation. However, the obtained values were still higher than the standard values. The below photograph shows the elongated length of all failed samples. It is evident that the elongated length of corroded samples (T4, T5, and T6) is lesser than the elongated length of un-corroded samples (T1, T2 and T3).

Figure 17. Photograph for the elongated length of all tensile samples after test.

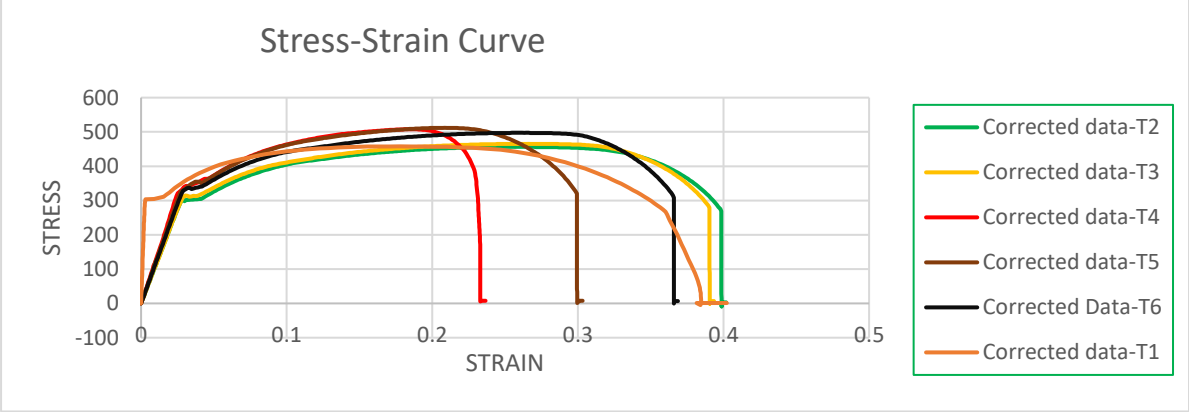

Figure 18. Stress-strain graphs of all tensile samples.

4.1.1. Discussions on the tensile results: Based on the observed results, the loss in yield and tensile strength is evident in all samples (corroded or non-corroded). In wet H_2S environments, the H^+ ions combine with the electron released by the corrosion of piping and form atomic hydrogen. More active corrosion will yield more atomic hydrogen on the surface of the piping exposed to the sour service. In general, atomic hydrogen can recombine to form molecular hydrogen, which is usually harmless for steel. But this atomic hydrogen

recombination reaction rate is significantly reduced due to the presence of H_2S. Thus the accumulated atomic hydrogen on steel surface can permeate into the steel material and gets accumulated at available hydrogen traps (inclusions/ grain boundaries/laminations/dislocations, etc.). This permeation of atomic hydrogen is directly proportional to the partial pressure of H_2S in the service [14-16]. The samples tested during this research have been operated at 80 bar pressure, with 3 mol% of H_2S in the liquid phase. This accumulated hydrogen can promote dislocation emission, multiplication, and motion at the local hydrogen enrichment region [17]. Another effect of hydrogen is to decrease the cohesive strength of Fe-Fe bonds. Finally, yet importantly, accumulated atomic hydrogen can recombine and form molecular H_2 and thus increasing the internal pressure, which can enhance the crack growth and thus reduction in both yield and tensile strength [2].

Another important observation made from the tensile testing was that "corroded samples" showed relatively lesser % elongation when comparing to non-corroded samples." Corroded samples were not polished and had pitting at the center of the reduced cross-sectional area of the tensile samples. Pitting can act as a stress concentration site and thus can affect the overall elongation of the corroded samples though overall, all samples revealed higher % elongation than the minimum required (17.5%) as per standard. The other main reason for this relatively lower elongation % in the corroded samples could be due to bulk material degradation (both macroscopic and microscopic) due to combining the effect of stresses and corrosive environment [3]. The charged hydrogen can significantly increase the dislocation density, thereby increasing the strength and reducing the % elongation in corroded samples when comparing with non-corroded samples.

The area under stress strain-curve in Figure 15 clearly shows a reduction in the toughness of the corroded samples.

4.2. Impact results

All samples were tested using Avery-Dension, UK –Impact Testing machine. Samples (I4 and I5) without notch were not broken, and the energy absorbed was significantly higher than the samples which were having a notch. Table 7 provides a summary of results:

Table 4. Absorbed energy (as per Charpy test) for the tested samples.

Sample Number	With Notch/WO Notch	Absorbed energy (Joules) @ Room Temp.	Avg. Absorbed energy for new API-5L-X60 material @ Room Temp
I1	Standard samples with Notch	60	1. 210.271 Joules [19] 2. 169 Joules [20] 3. 260 [at 50 deg C, as per material test certificate of new API 5L-X60 material]
I2		61	
I3		60	
I4	Corroded samples with pitted area at the center (No notch)	102	
I5		102	

Figure 19 shows the broken Impact samples. It is evident that the samples without notch did not break and absorbed more energy. Additionally, the notched samples were not broken into two pieces. However, as per ASTM standard-E23- "If a fractured impact specimen does not separate into two pieces, report it as unbroken. Unbroken specimens with absorbed energies of less than 80 % of the machine capacity may be averaged with values from broken specimens."

Figure 19. Photograph for the Charpy specimens after the test.

4.2.1. Discussions on the impact testing results: Significant decrease in brittle fracture resistance (absorbed energy) at room temperature was noticed in all tested samples. This may be explained by the presence of hydrogen (produced due to corrosion) mostly bound in deep traps, inclusions sites available in the original material. During the impact tests, the diffusion and accumulation of hydrogen were inhibited due to high impact speed. The reduction in the Charpy absorbed energy of specimens after corrosion can be mainly attributed to the decreasing Fe-Fe bonds and the presence of hydrogen-induced microcracks [6]. Similar kinds of results were also reported by researchers while testing an in-service material X52 Steel [3].

4.3. XPS Results:

All the tested samples (A1/A3/B1/B3) showed the presence of sulphur, iron and oxygen in the surface analysis results. Table 8 provides the summary of elements found in each tested sample:

Table 5. The atomic concentration of various elements in tested specimens.

Sample No.	Element atomic concentration					
	Sulfur	Fe	Oxygen	Carbon	Cu	Zn
A1	6.93	3.39	10.52	68.36	8.48	0.19
A2	16.94	5.98	10.98	49.38	13.36	0.15
A3	18.48	5.31	11.82	53.09	10.34	0.69
B1	11.46	3.68	13.4	58.81	9.74	0.35
B2	5.1	3.34	12.88	72.21	4.67	0.4
B3	1.85	1.57	7.45	88.72	0.29	0
B4	7.39	2	11.72	71.86	5.01	0.23

4.3.1. Discussions on XPS results: Peek fitting of XPS data (Refer Fig-20 & 21) shows the presence of hydrocarbon, iron oxides, iron sulfide, and iron sulfite, and elemental sulfur. The presence of elemental sulfur explains the yellowish layer observed in the corroded samples during visual inspection. Glycol was injected in the piping during every winter season to inhibit hydrate formation, which can explain the presence of hydroxide in deposits. The presence of elemental sulfur in a sour environment makes it very aggressive for corrosion [21].

Elemental sulfur is generally present in the sour gas coming from offshore and is produced due to oxidation of H_2S. Like the temperature, the pressure of the pipeline changes, the elemental sulfur can get accumulate on the pipe surface and can cause catastrophic corrosion of carbon steel [22]. The corroded pipe taken for this research is a dead leg (a portion of pipe with no flow/ intermittent flow), and thus conditions are ideal for the elemental sulfur deposition. Formation of elemental sulfur can take place in an aqueous system, as a result of

the oxidation of sulfide species, as shown by following equations [23]:

$8\ H_2S\ (aq) + 16\ M^{n+}\ (aq) \longrightarrow 16\ H^{+}\ (aq) + 16\ M^{(n-1)+}\ (aq)$ Equation (1)

$8\ H_2S\ (aq) + 4\ O_2\ (g) \longrightarrow S_8\ (s) + 8\ H_2O\ (l)$ Equation (2)

Some researchers have proposed that the formation of acidic species due to the hydrolysis of sulfur species is the governing factor for corrosion in the presence of elemental sulfur [24]. Other researchers hypothesized that an electrochemical reaction between iron and polysulfide is the driving force for corrosion in systems with the presence of elemental sulfur [25-26]. Though consensus has not been reached in terms of actual corrosion mechanism related to the elemental sulfur, recent experiments done to quantify the effect of element sulfur on corrosion rate, concluded that the absence of sulfur decreases the corrosion rates by two-fold and thus proving that even 1 ppm of elemental sulfur can be a significant contributor to higher corrosion rates [21].

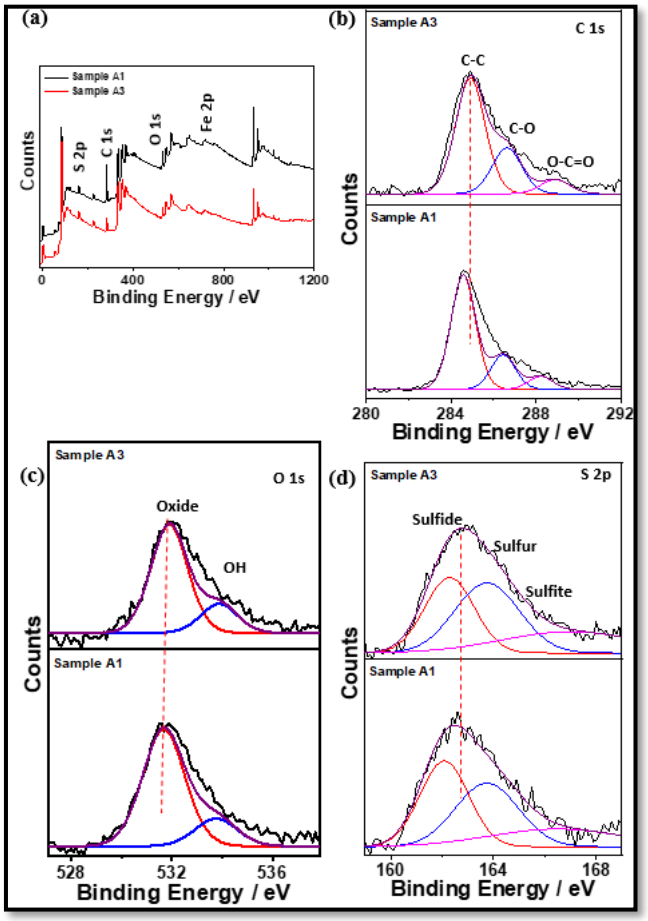

Figure 20. XPS –peak fitting for samples A1/A3-a) full survey, b) carbon;

c) oxygen and d) sulfur

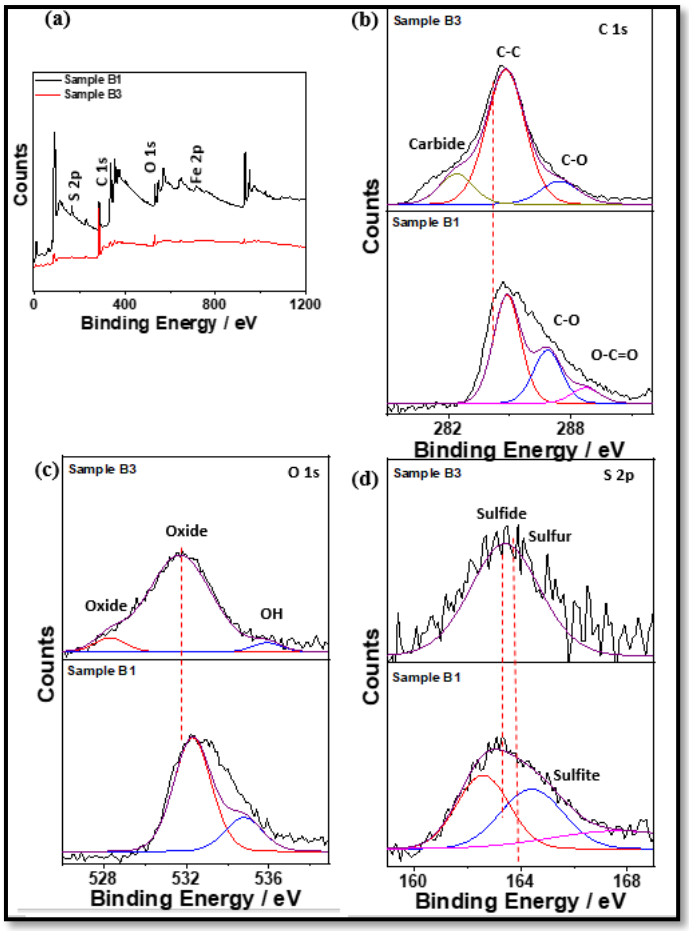

Figure 21. XPS peak fitting for samples B1/B3-a) full survey, b) carbon;

c) oxygen and d) sulfur

4.4. SEM/EDS RESULTS:

All samples were analyzed with SEM/EDS technique, to understand the as-received surface morphology of the corroded as well as non-corroded samples. All analyses showed a significant presence of sulfur in deposits. Following figures (22-35) shows the EDS analysis and sample SEM image of all tested samples.

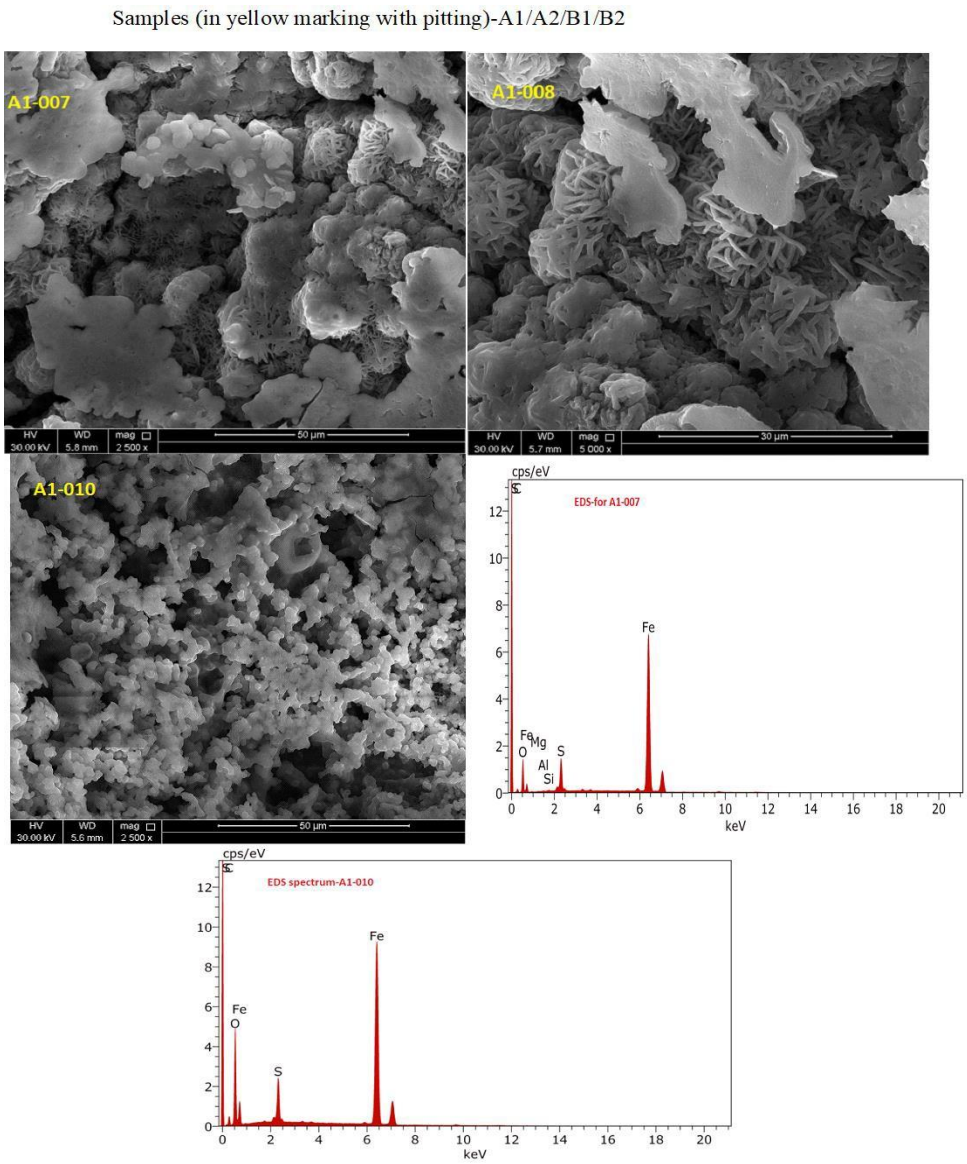

Figure 22. The SEM micropgraphs and the EDS analysis for Sample-A1.

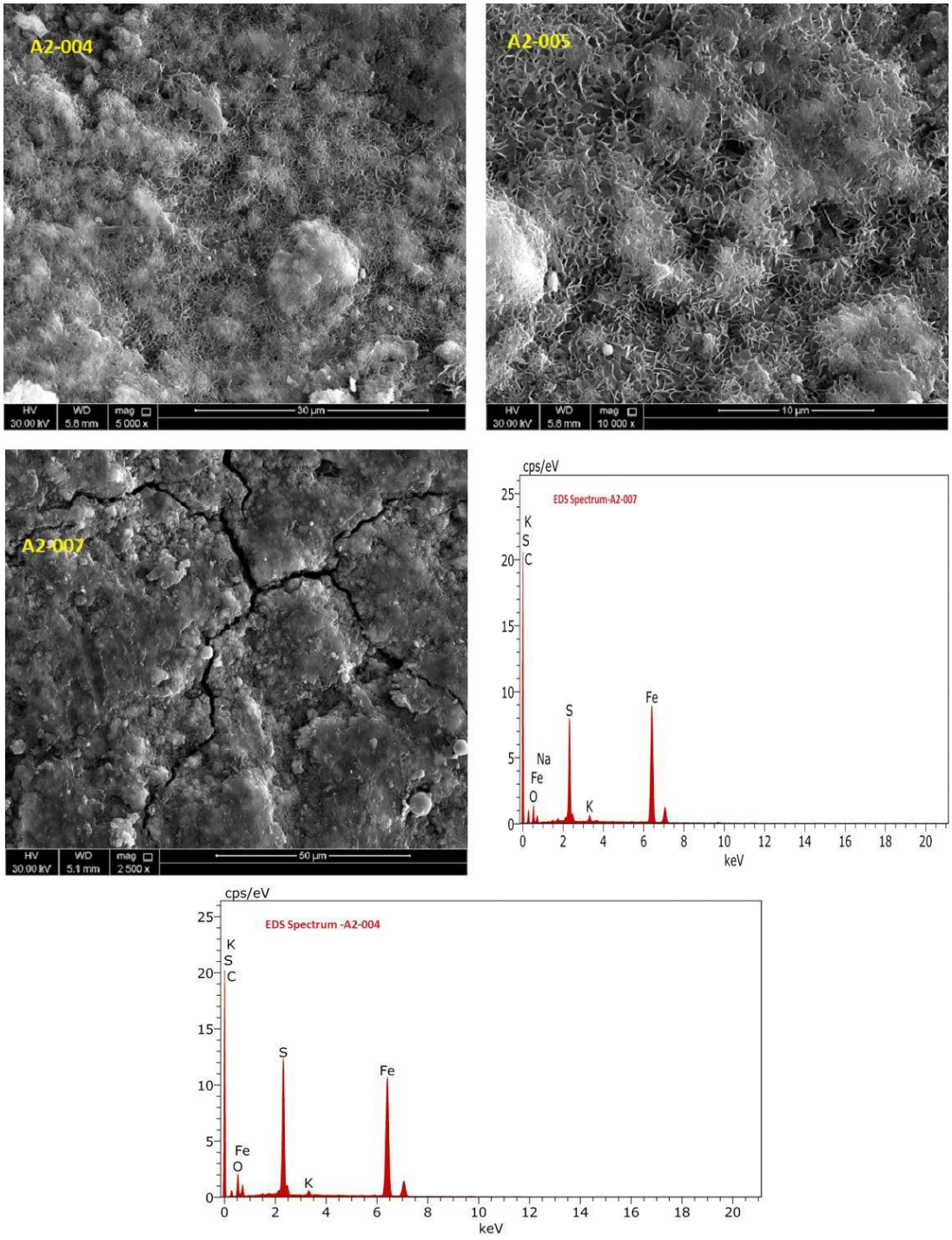

Figure 23. SEM images (Sample-A2) showing porous nature of corrosion scales.

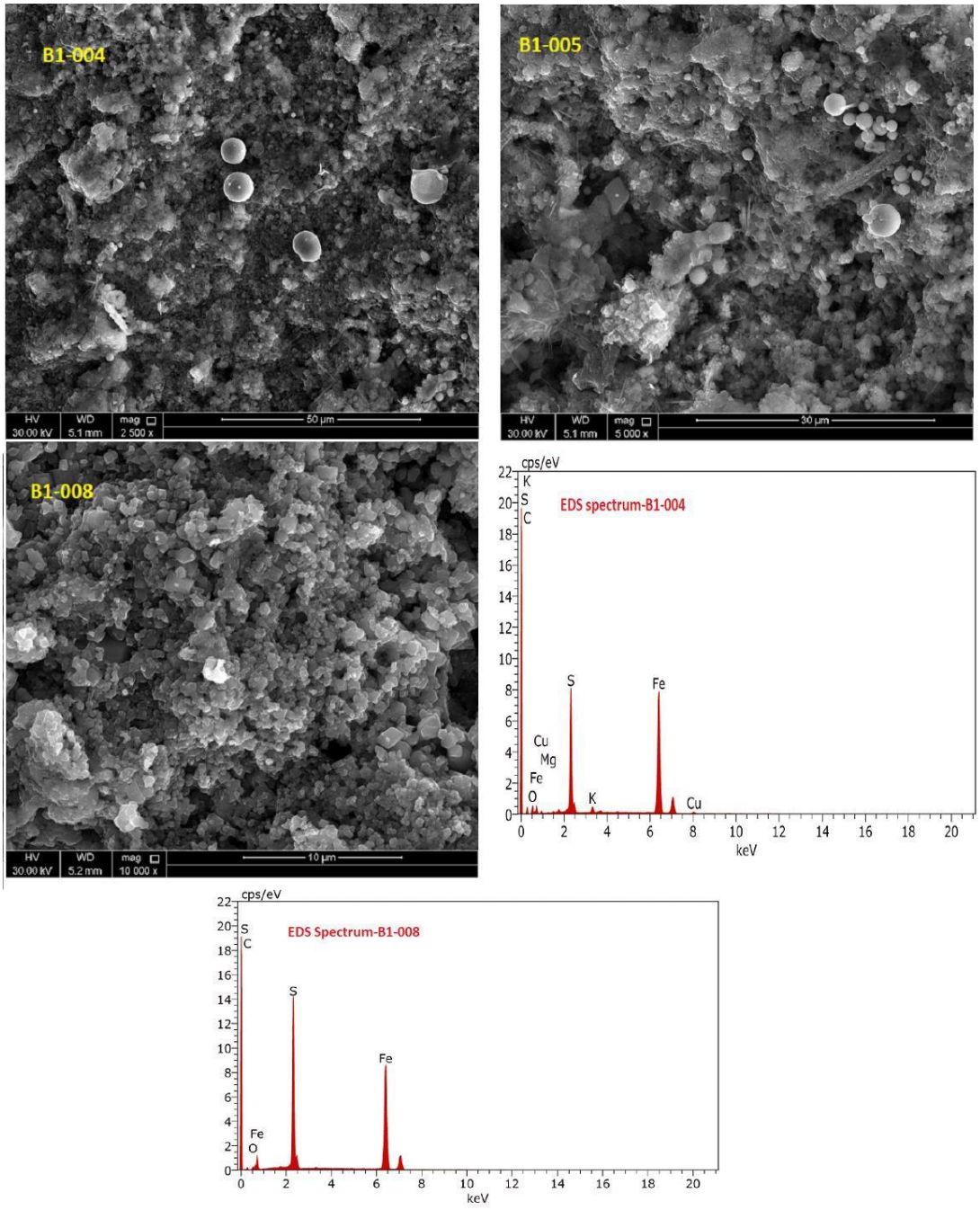

Figure 24. SEM images (B1) showing close up view of scales/ EDS analysis confirming presence of Sulfur.

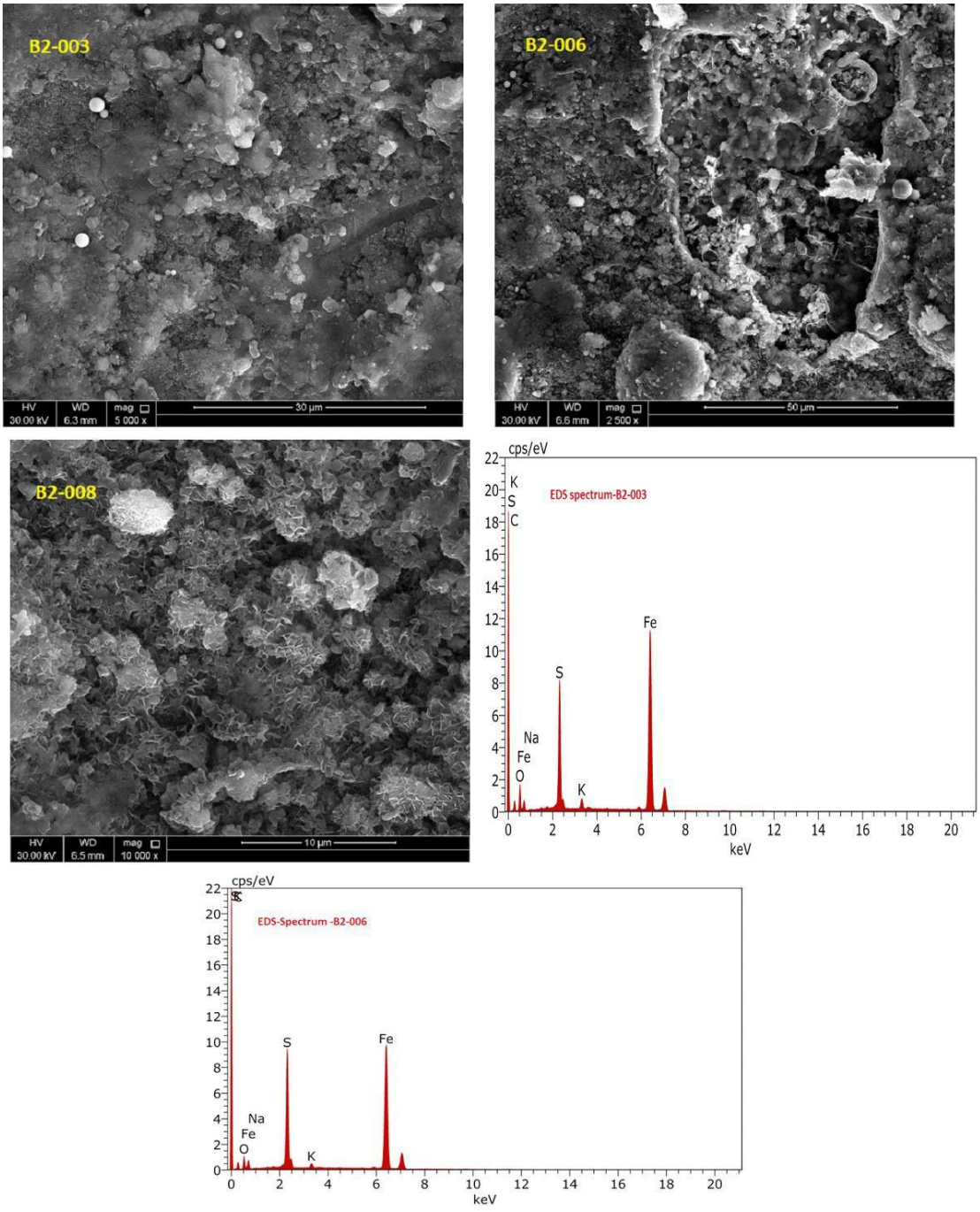

Figure 25. SEM and EDS analysis for Sample-B2

SAMPLES WITH PITTING (OUTSIDE YELLOW MARK AREA) -(A3/B3/B4)

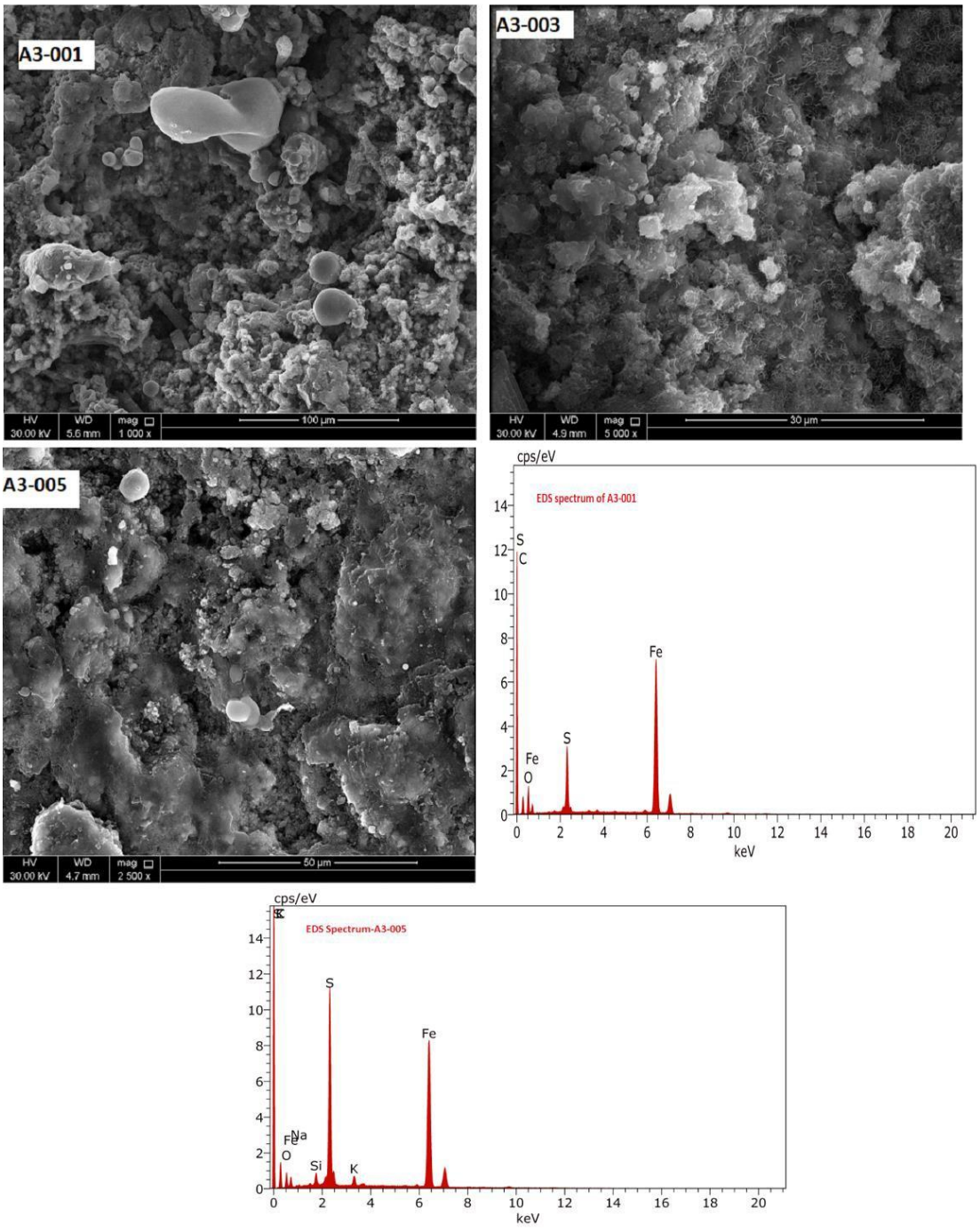

Figure 26. SEM and EDS analysis for Sample-A3.

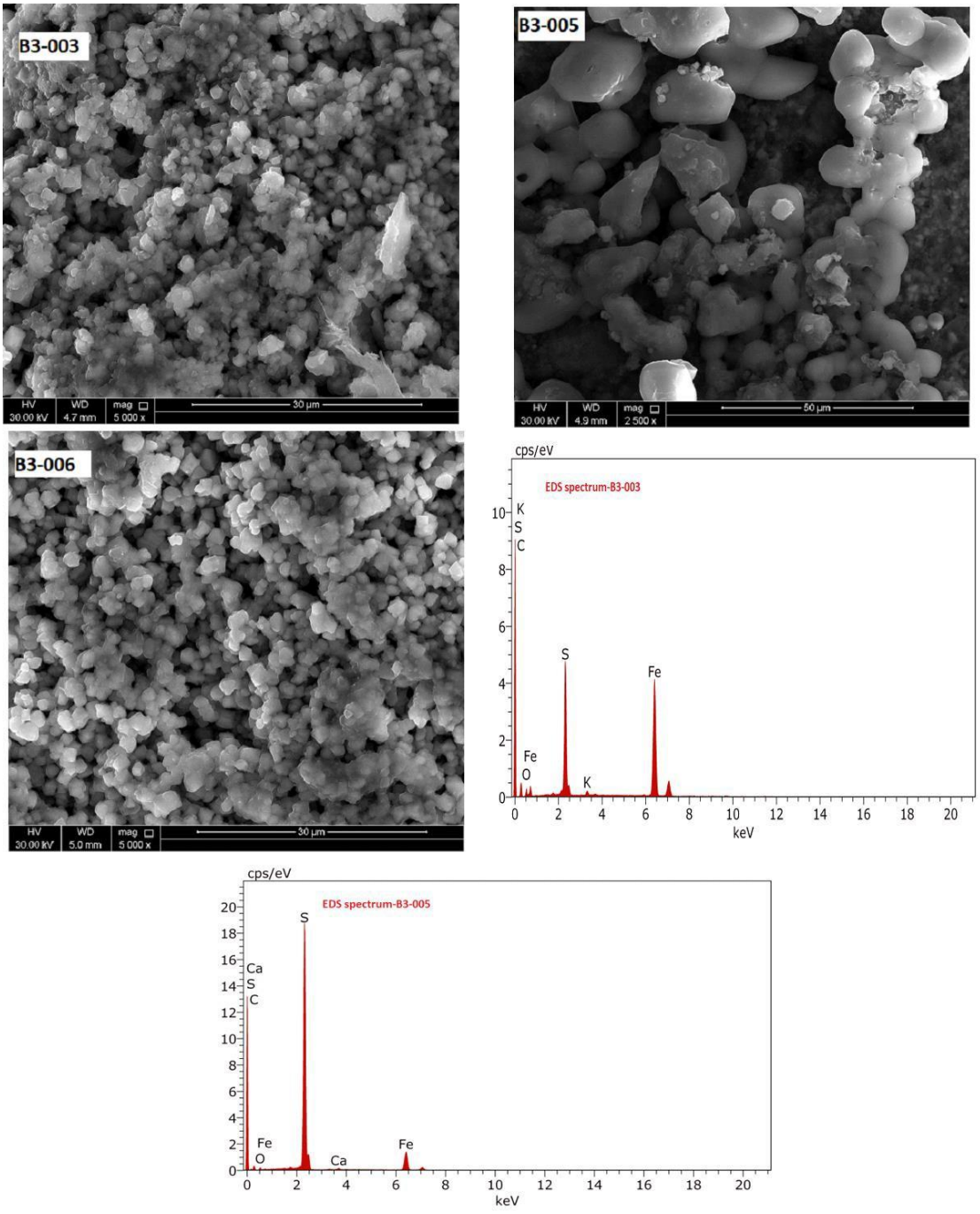

Figure 27. SEM images showing sulphur grains/ EDS analysis for Sample-B3.

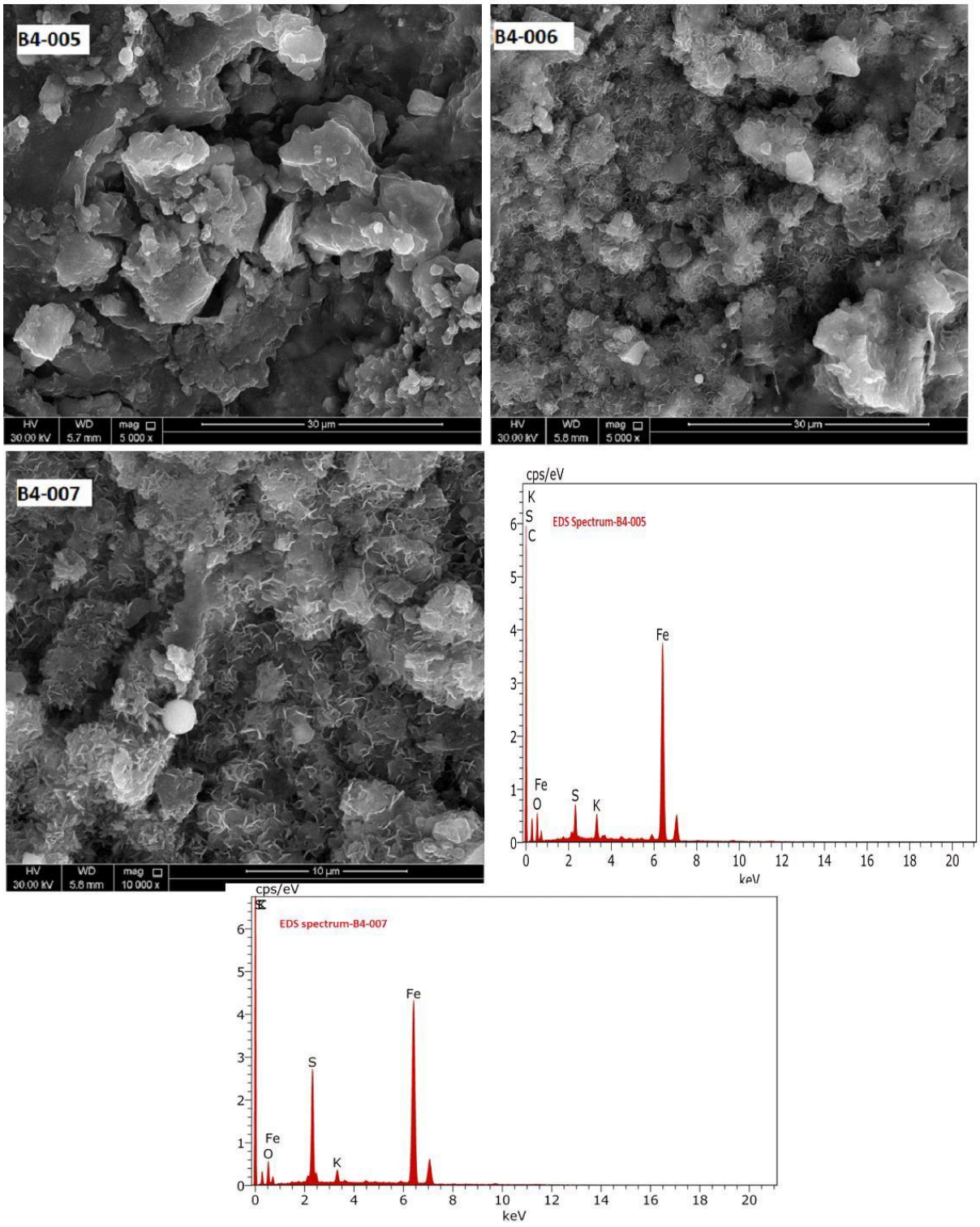

Figure 28. Showing SEM and EDS analysis for Sample-B4.

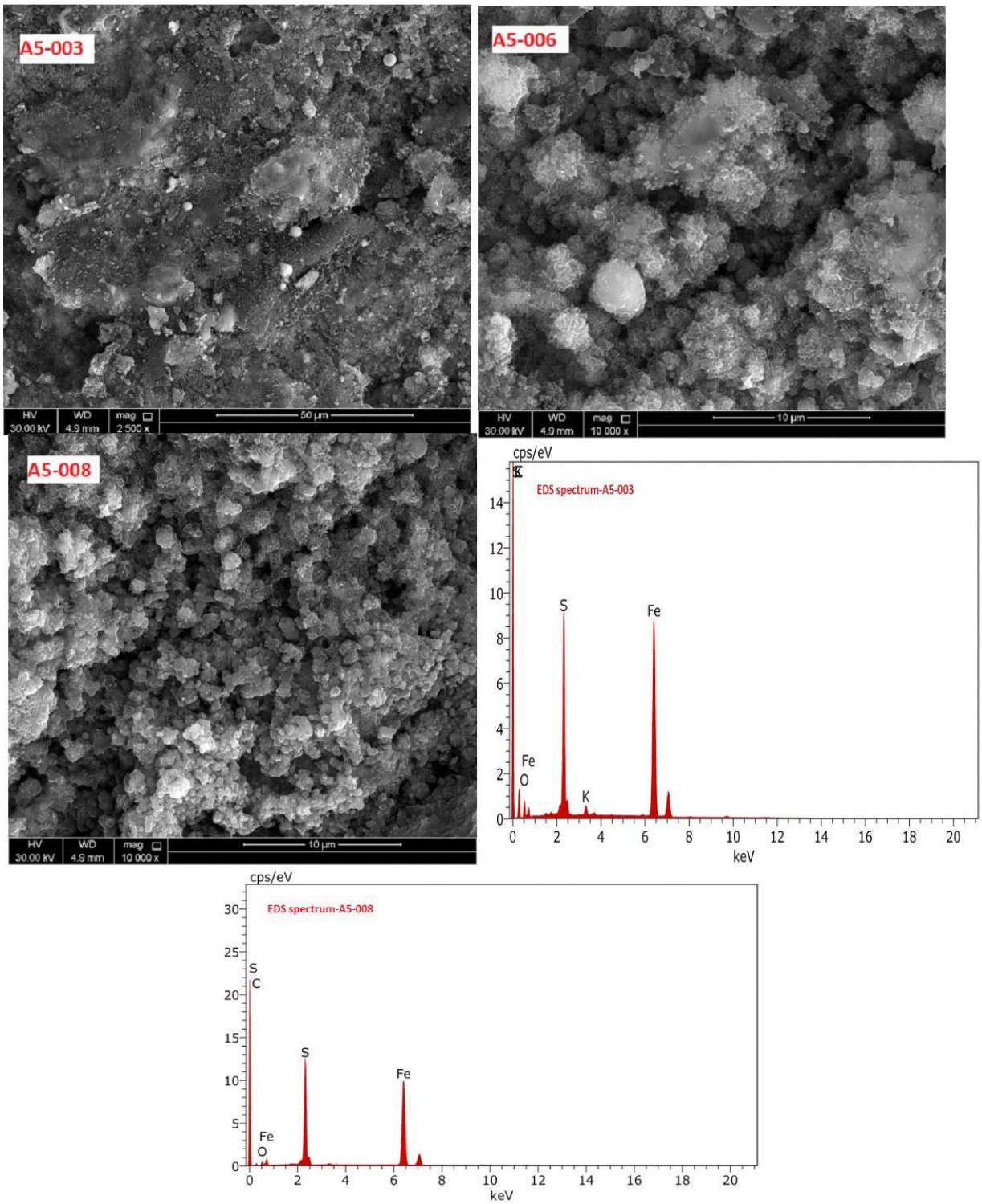

Figure 29. SEM and EDS analysis for Sample-A5.

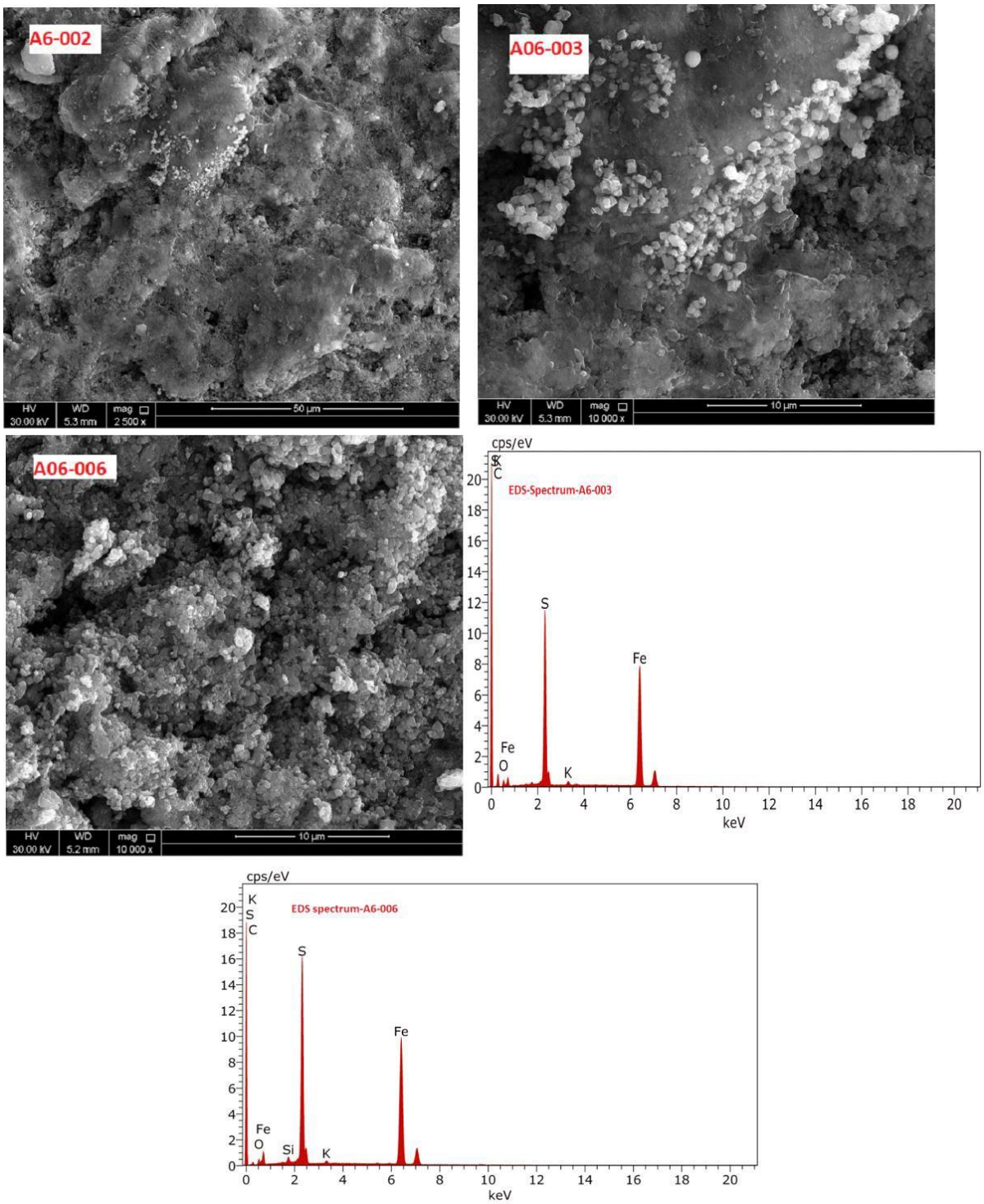

Figure 30. SEM and EDS analysis for Sample-A6.

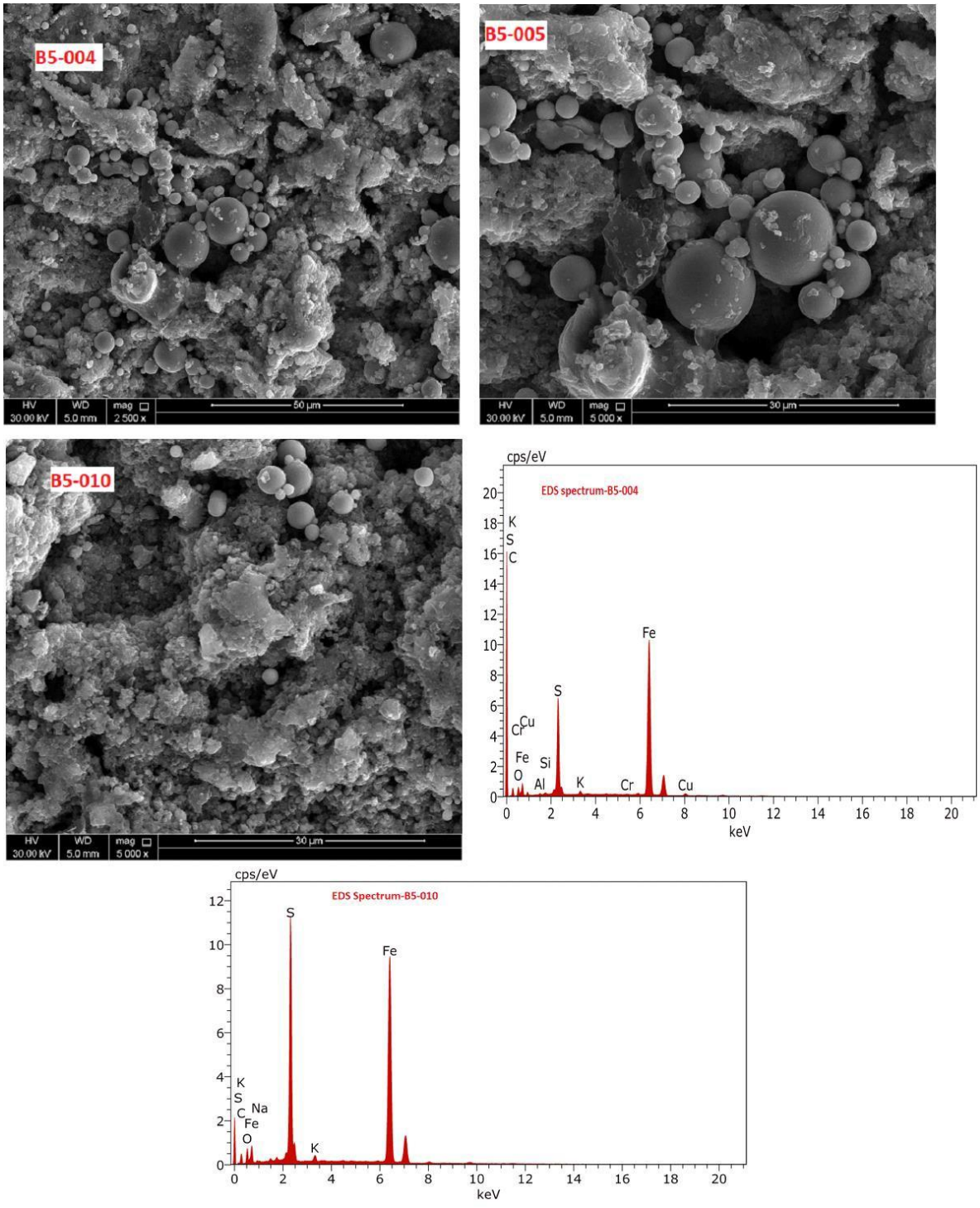

Figure 31. SEM images (Top-Right) showing speherical mineral agregate (B5)

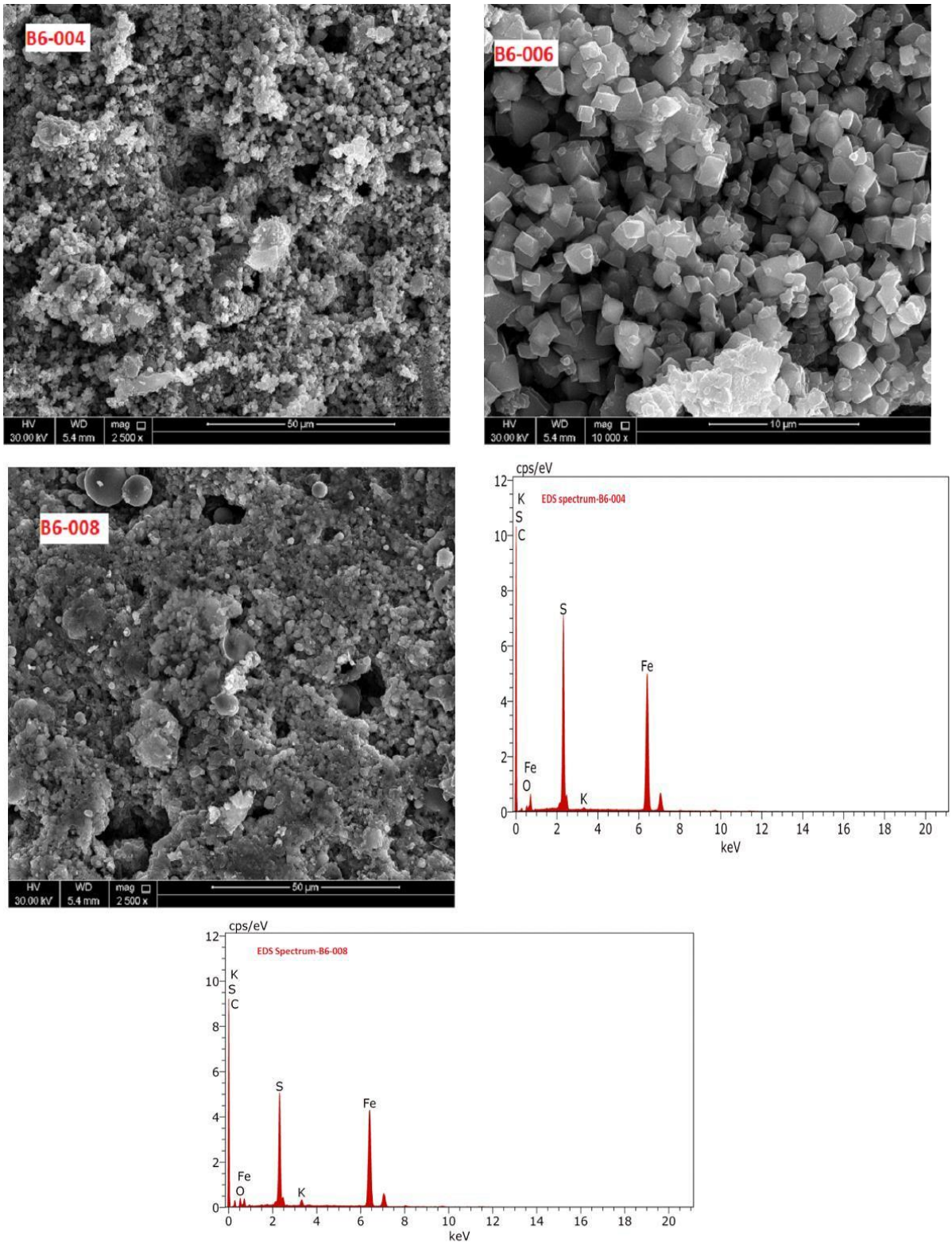

Figure 32. SEM images (Top Right) showing posible Sulphur grains.

4.4.1. Discussions on SEM results: The above-shown SEM micrographs were taken without any cleaning or polishing to understand the pitting/corrosion morphology and to carry out deposits analysis. Samples were divided into three categories:

a. Samples with pitting in the yellow mark area (A1/A2/B1/B2)- Fig-19 to Fig-22 show the SEM images and EDS analysis of these samples.
b. Samples with pitting, outside yellow mark area (A3/B3/B4)-Fig-23 to Fig-25 provides the SEM images and EDS analysis of these samples.
c. Samples with no evident pitting (A5/A6/B5/B6)- Fig-26-Fig-29 provides the SEM images and EDS analysis of these samples.

Carbon, Fe, elemental sulfur, Na, K were found in all EDS analysis. The corrosion deposit layer was found porous (non-adherent) with multiple cracks, which indicates active corrosion. Samples with visible pitting were also seen with corrosion products similar to the one found in pitted samples. SEM images clearly indicate active corrosion happening in the piping.

4.4.2. SEM analysis of tensile sample fractured surface: Two tensile samples (corroded and non-corroded) were examined with SEM to understand the difference of failure mode of corroded and non-corroded samples. Fig-33 shows SEM images at 2500 x, 5000x, 1000x and 20000x of both the samples. Significant differences can be noticed in the failed tips. Micro-voids or crack can be seen in sample-T4(Corroded). The depth of the cup/cone is significantly more in the T2 sample (non-corroded). Thus indicating that active corrosion has impacted the ductility and microstructure of the piping material. The same was noticed in terms of the elongation% results.

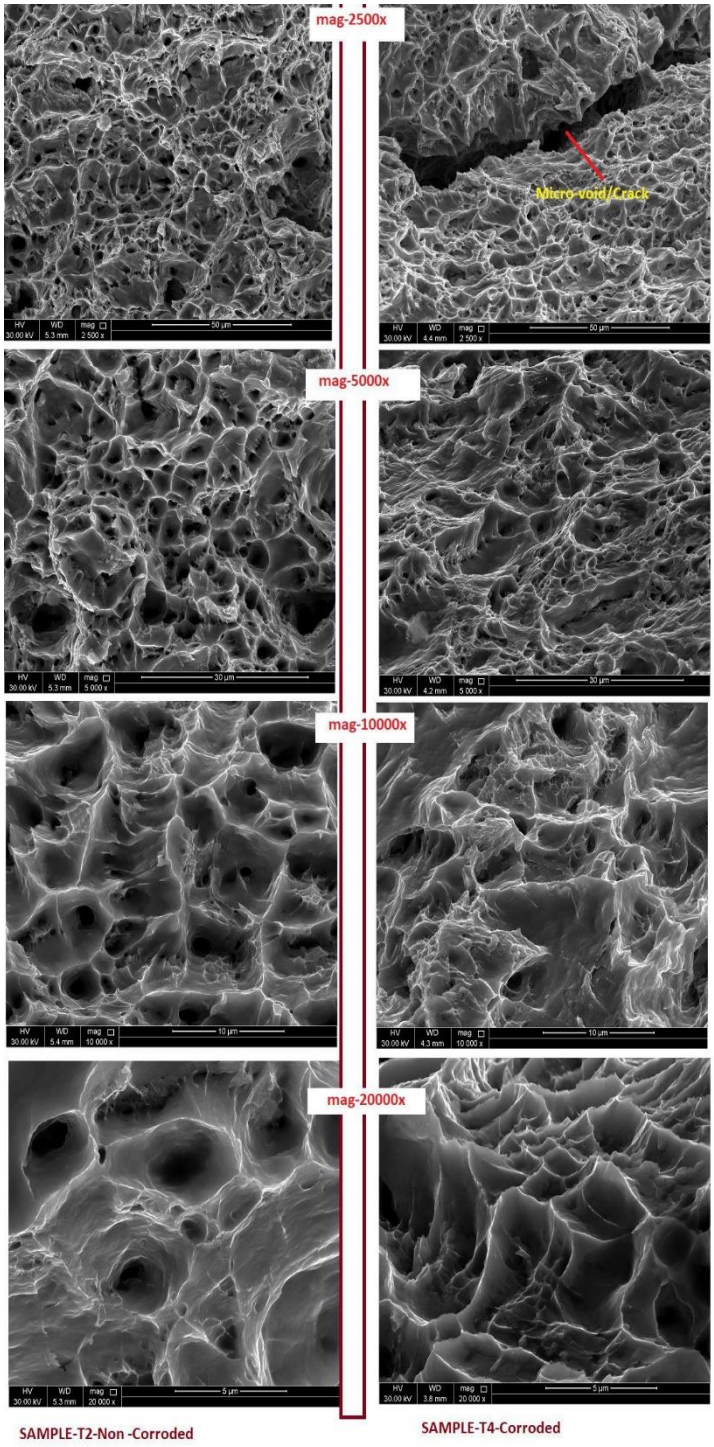

Figure 33. SEM images for failed T2 (Left) and T4 (Right) Tensile samples.

4.5. Microhardness Results:

As mentioned above, two corroded samples were polished, and microhardness was taken across the cross-sectional area to understand the difference in hardness from ID to OD of the samples. Below photograph shows, one of the samples and hardness profile was developed from ID to OD, i.e., from the corroded surface to the bulk material.

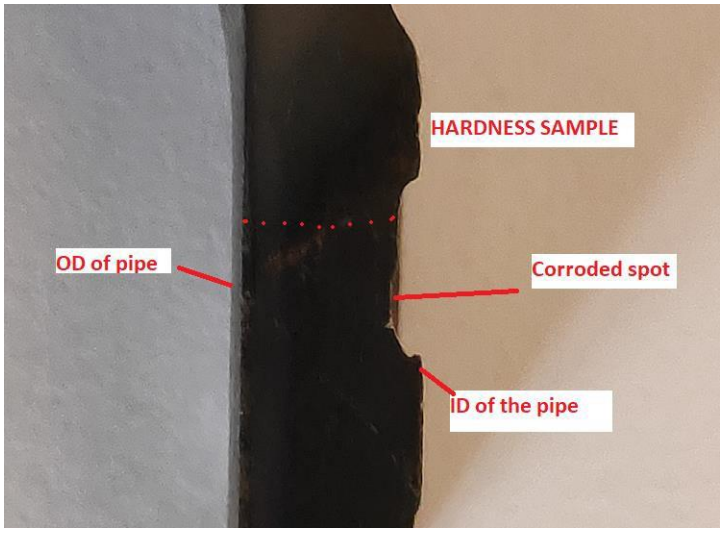

Figure 34. Image for one of the tested hardness sample.

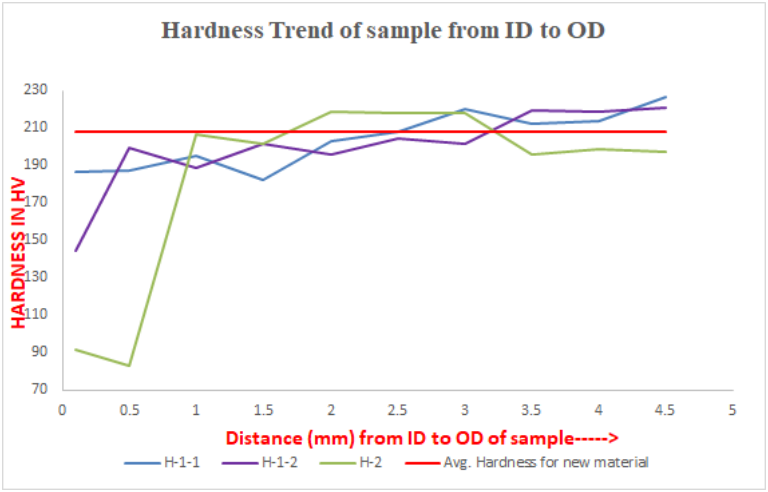

Figure 35. Hardness results of samples-H1 and H2.

4.5.1. Discussions on hardness results: From the hardness data, the low thickness is evident at the ID (near the corroded surface) of the samples. Hardness in the bulk material (at center and OD) is observed similar to the average hardness of new API 5L-X60 material. Loss of hardness is aligned with yield strength, and UTS results got from these samples. This indicates the effect of prolonged in-service environment and active corrosion. The overall mechanical results can be summarized as-loss of strength, and toughness, accompanied by a reduction in hardness (especially at the exposed surface). Similar results were reported by H. Nykyforchyn et al. , and the results were explained by the proposed theory of the development of microdefectness, after 10-20 years of service [3].

4.6. Optical Microscopy Results

The samples, which were used for hardness testing, were also examined by optical microscopy to understand the difference in microstructure at the ID and bulk of the sample. Optical microscopy images (see Figure 36) clearly indicate differences in microstructure at the area exposed to service (Sample ID) and at the bulk of samples. The cluster of hydrogen blisters can be seen near the ID of corroded samples. The area near the ID/corroded surface also corresponds to low hardness. The presence of micro-cracks near the ID of the sample is also clearly visible. These findings clearly indicate significant degradation in the material due to long-term exposure in sour service.

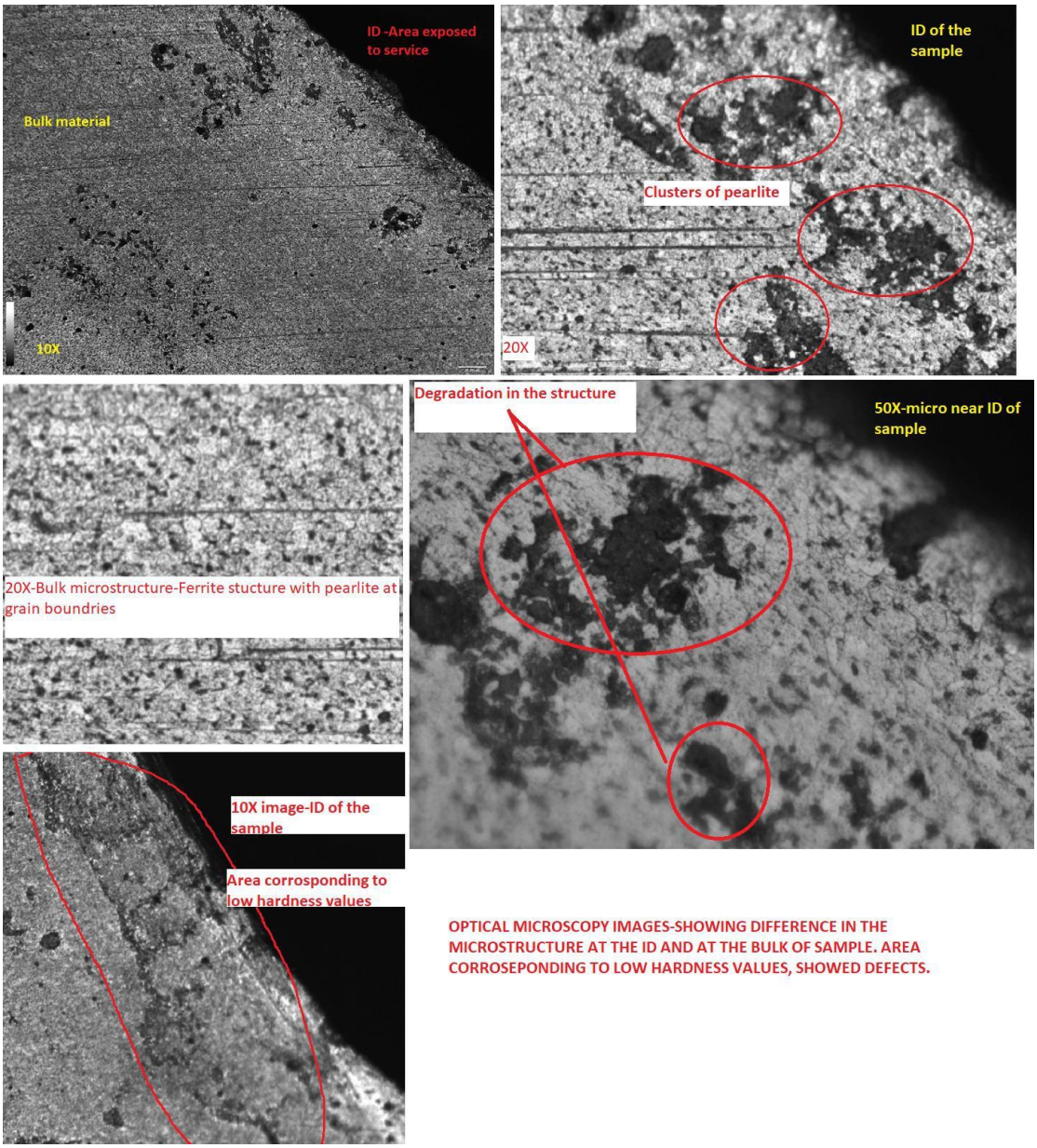

Figure 36. Optical microscopy images at the various mag, for both ID and bulk.

4.7 Electrochemical Impedance Spectroscopy (EIS)

EIS technique has been employed to describe the electrode/electrolyte interfaces quantitatively. It is considered as a potent method that can explain the corrosion behavior and calculate their rates. Figure 35 shows the proposed equivalent circuit (EC) utilized to analyze and fit the collected experimental data. Figure 35 exhibit the one-time constant equivalent circuit, which is commonly used for analyzing electrodes undergoing uniform corrosion. The parameters of the electrochemical reactions occurring at the metal/solution interface are listed in Table 9 and measured and calculated from the EIS Nyquist and bode plots, in which the electrolyte resistance (R_s), charge transfer resistance (R_{ct}), constant phase elements for the charge transfer resistance (CPE_{ct}), and the deviation parameters (n) from the ideal double-layer capacitance (C_{dl}) are listed.

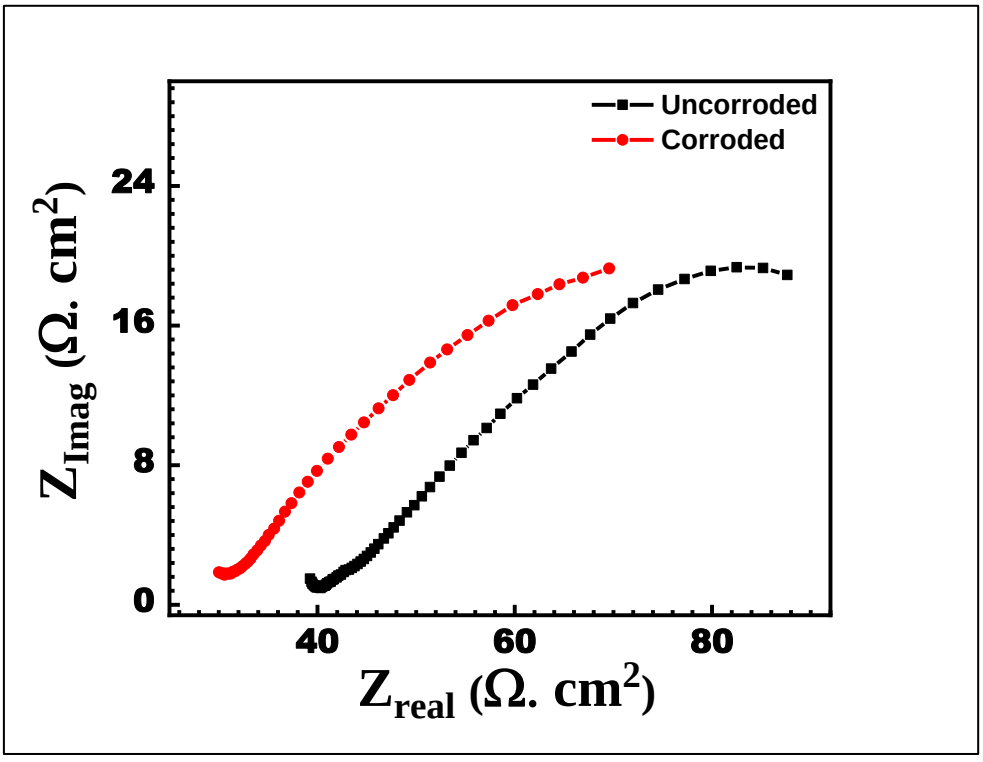

Figure 37. Nyquist plots for the measured EIS data (dots) for non-corroded (black) and corroded (red) API-5L-X60 specimens immersed I 0.5 M Na_2SO_4. The solid lines are the fitted curves.

The constant phase element is used in place of a pure capacitor as it is composed of the capacitance and deviation parameter to encounter the imperfectness behavior of a double layer, which may occur because of a non-uniform thickness of the corrosion inhibitor layer, non-uniform corrosion reaction on the surface, or non-uniform current distribution and surface roughness. The capacitance behavior is mainly attributed to the dielectric nature of the surface film (corrosion product and/or inhibitor film) which affects the corrosion rate of the metal, and it can be expressed by the following Equation[27]:

$$\mathbf{Z_{CPE} = [Y_0^{-1}\ (j\omega)^{-n}]} \qquad \text{Equation (3)}$$

where Z_{CPE} is the impedance of *CPE* (Ω cm^{-2}), Y_o is a proportional factor in s^n Ω^{-1} cm^{-2}, $j = (-1)^{1/2}$, ω is the angular frequency in rad s^{-1} and n is the deviation parameter, and its value is between 0 and 1. When n = 1, the *CPE* becomes equivalent to an ideal capacitor, and when $n = 0$, the *CPE* becomes equivalent to a resistor.

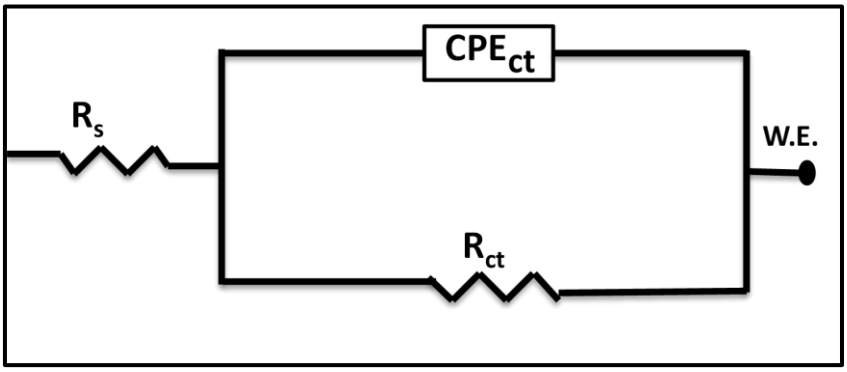

Figure 38. Equivalent circuit (EC) used to fit the measured data.

Table 6. EIS Parameters for the two C-steel samples tested in 0.5 M N_2SO_4.

Sample Type	R_s, Ω cm^{-2}	*CPE1* $\times 10^{-6}$ $s^n\ \Omega^{-1}$ cm^{-2}	n_1	R_{ct}, Ω cm^{-2}
Uncorroded	40.21	478	0.568	98.11
Corroded	27.22	946	0.598	64.63

4.7.1. Discussions on Electrochemical results: Figure 37 and Table 6 clearly show that the corroded sample (without polishing) exhibit lower corrosion resistance when compared to the un-corroded polished sample. This also proves that the corrosion product layer on the corroded sample is not adhered and is not sufficient to stop further corrosion. These results are also aligned with SEM images results, which showed the porosity in the corrosion deposits, found in the samples.

4.7.2. Correlating results of XPS/SEM/EDS/Optical microscopy and EIS Testing:

The SEM images of the pitted as well as not pitted samples, showed a significant amount of porous deposits. Corrosion impacts the generation of atomic hydrogen, which can diffuse into steel and get accumulates and form blisters as seen in the optical microscopic images. The process parameters of the failed sample show the presence of sulfides, carbide and free sulfur thus making it a complex system to predict corrosion rates [28]. A lot of research work and studies have been undertaken to understand the effect of H_2S in the CO_2 system [29-33]. The corrosion process involves lots of complex combination of reactions which affects the corrosion rates and film-forming rates. In the presence of aqueous H_2S, iron sulfide formation can take place by any of the three routes. First is the formation of the blackish layer by the anodic dissolution of iron at the surface. This Fes layer/film keeps on increasing by continuing anodic dissolution of iron at the metal and sulfide film interface. However, the reaction rate is limited by the diffusion of Fe ions and electrons through the FeS layer. Another possibility is that Fe ions directly dissolves into solution and react with sulfide ions present in the solution. No FeS layer is deposited on the solution/metal interface during this kind of interaction. The third possibility is the combination of the above two explained reactions, where ferrous ions react both at the surface and the solution, thus causing the formation of porous, non-adherent, and non-protective FeS layer. This porous corrosion layer supports cathodic reaction along with creating anodic dissolution of Fe [34-35].

As explained in section 4.3.1, the presence of elemental sulfur can further aggravate the corrosion rates. The above results indicate that the corrosion product layer observed in the examined samples is porous, non-adherent, and thus providing no protection against ongoing corrosion.

4.7.3. Correlating mechanical and SEM/EDS analysis.

Results obtained from all the mentioned testings need to be analyzed comprehensively, with respect to the overall effect of the hydrogen charging environment on the material properties. Material strength has been reduced, along with an increase in elongation%. Similarly, hardness values were reduced at the ID of material, which was exposed to the sour service along with a significant reduction in the absorbed energy values during the impact testing. SEM analysis of the fractured surface of tensile samples clearly indicates the presence of microvoids/microcracks. The size of dimples was found smaller in the corroded sample as compared to non-corroded samples. All of these changes can be attributed to the effect of hydrogen charging in the material due to prolonged exposure of wet H_2S service. Based on previous researches, there are mainly three principal mechanisms of hydrogen embrittlement (HE) and Hydrogen induced sulfide stress corrosion cracking, which can be used to explain the observed results during this research. These are Hydrogen Enhanced Localized Plasticity (HELP), Hydrogen Enhanced DEcohesion (HEDE), and Adsorption Induced Dislocation Emission (AIDE) [36].

HELP: This mechanism is based on the localized softening because of the solute hydrogen forming hydrogen atmosphere around both mobile dislocations and dislocations obstacles [37]. This results in the reduction of resistance of dislocation motion due to obstacles and increment in the dislocation velocities in the presence of hydrogen. As the hydrogen concentration is localized near crack tips due to hydrostatic forces, it is proposed that deformation is facilitated locally near crack tips via a localized microvoid coalescence process. Thus, HELP should result in smaller dimples on fracture surfaces than those produced in inert environments [36].

HEDE: This mechanism is based on the weakening of metal-metal bonds at or near crack tips due to the high concentration of hydrogen, resulting in tensile separation of atoms in place of slip [38-45]. “The weakening of bonds is thought to result from a decrease in electron charge density between metal-metal atoms owing to the presence of hydrogen” [36].

AIDE: This mechanism is also based on the weakening of interatomic bonds due to hydrogen charging, causing crack growth by localized slip instead of tensile separation [46]. It has been proposed that the adsorbed hydrogen (at the surface and up to few atomic layer depths) causes weakening in the interatomic bonds of the substrate, further facilitating the emission of dislocations from the crack tip.

Considering the complex nature of the mechanism explained above, it is extremely difficult to conclude one mechanism causing an alteration in the mechanical properties of the material. These mechanisms for cracking may occur conjointly in some circumstances, although with one dominant mechanism [36].

However, all the above cracking mechanism (or their combination) can explain the reduction in the strength of material and increment in the elongation%. The effect of adsorbed hydrogen near the ID may also cause the softening effect of the substrate.

CHAPTER 5: CONCLUSION

The purpose of the research was to understand the effect of prolonged exposure of sour environment on the piping material (API-5L-X60), which was selected as per NACE-MR0175 standard. Limited research has been done on the piping samples that have been exposed to the severe sour environment. Tensile test results clearly suggest the degradation of material in terms of 22% reduction of yield strength and a 5% reduction of UTS as compared to the minimum standard values. Reduction in YS and UTS was also accompanied by an increase in elongation%. A clear difference was observed in the corroded and non-corroded samples in terms of % elongation, with corroded samples demonstrating 10-15% less elongation. Moreover, the overall toughness of the corroded samples was also observed significantly lower than the un-corroded samples. Additionally, severe reduction (64%) in the impact properties was also observed in the samples, proving that prolonged exposure has significantly reduced the impact toughness of the piping material. Hardness data revealed a difference near the exposed surface (ID) against that at the bulk of the material. The surface exposed to sour service exhibited lower hardness values compared to bulk hardness. Optical microscopy also revealed degradation in microstructure near the ID of the pipe. Hydrogen blistering and microcracks can be clearly seen in optical microscopy images at the ID of the samples. EIS data also proved that the corrosion deposit layer is not adhered to the C-steel surface, and also it is porous and hence not enough to stop further corrosion. The corrosion resistance of corroded samples was observed significantly lower than the corrosion resistance of the fresh sample.

The research confirmed the degradation of pipeline steel (with active corrosion) over a period of 15 years of service. Impact of active corrosion is not limited to reduction in thickness; rather it had also impacted the critical mechanical properties of the material.

CHAPTER 6: FUTURE WORK

The selection of material for any sour service is currently being made on the basis of established international standards like ISO15156 (NACE-MR0175). However, no guideline has been established to confirm the continuing suitability of the selected material after prolonged exposure to sour service. This requirement is especially important for the piping exhibiting active corrosion. Further research is required to examine the exposed materials as per NACE testing standards (NACE-TM- 0284/T177) and to confirm their suitability for the continuous service. Hydrotest requirement during partial piping replacement projects needs to be carefully evaluated, considering significant reduction in mechanical properties of the exposed material. Exposing such material to hydrotest pressure may result in propogation of pre-existing micro-cracks/micro-voids in the exposed steels. It is also proposed to install mechanical testing coupons, along with conventional corrosion coupons in critical sour service pipelines. Such coupon can be removed after specific time intervals, and mechanicaly tested to establish the rate of degradation, in such services.

REFERENCES

1. Timmins, P. F., & ASM International. (1997). Solutions to hydrogen attack in steels. Materials Park, OH: ASM International: p. 52-166
2. Qi, Yameng & Luo, Hongyun & Zheng, Shuqi & Chen, Changfeng & Lv, Zhenguo & Xiong, Maoxian. (2014). Comparison of tensile and impact behavior of carbon steel in H2S environments. Materials & Design: p. 234–241.
3. Nykyforchyn, H. & Lunarska, E. & Tsyrulnyk, O. & Nikiforov, K. & Genarro, M. & Gabetta, Giovanna. (2010). Environmentally assisted "in-bulk" steel degradation of long term service gas trunkline. Engineering Failure Analysis-ENG FAIL ANAL: p. 624-632.
4. NACE-SP0296-2016 (formerly RP0296), Detection, Repair, and Mitigation of Cracking in Refinery Equipment in Wet H2S Environments
5. ANSI/NACE MR0175/ISO 15156-Petroleum and natural gas industries—Materials for use in H2S-containing environments in oil and gas production.
6. Bich, N. N., & Goerz, K. (1996, January). Caroline Pipeline Failure: Findings on Corrosion Mechanisms in Wet Sour Gas Systems Containing Significant Co. In CORROSION 96. NACE International.
7. Bich, N. N. (2006). Corrosion Monitoring For Wet Sour Gas Pipelines. In CORROSION 2006, Paper 06642, NACE International.
8. Siegmund, G., Schmitt, G., & Sadlowsky, B. (2000, January). Corrosivity of methanolic systems in wet sour gas production. In CORROSION 2000. NACE International.
9. Xie, J., Yang, L., Worthingham, B., & King, F. (2009, January). Hydrogen

Effects On High Strength Pipeline Steels. In CORROSION 2009. NACE International.

10. Fassina, P., Bolzoni, F. A. B. I. O., Fumagalli, G., Lazzari, L., Vergani, L. A. U. R. A., & Sciuccati, A. (2012). Influence of hydrogen and low temperature on mechanical behaviour of two pipeline steels. Engineering Fracture Mechanics, 81, p. 43-55.
11. https://en.wikipedia.org/wiki/Scanning_electron_microscope
12. https://en.wikipedia.org/wiki/Energy-dispersive_X-ray_spectroscopy
13. https://www.labtesting.com/services/materials-testing/metallurgical
14. Specification, A. P. I. (2018). 5L, Specification for Line Pipe. Edition March.
15. Chu, W. Y. (1988). Hydrogen damage and delayed fracture. Chinese Metallurgical Industry Press, Beijing.
16. Kawashima, A., Hashimoto, K., & Shimodaira, S. (1976). Hydrogen electrode reaction and hydrogen embrittlement of mild steel in hydrogen sulfide solutions. Corrosion, 32(8), p. 321-331.
17. Gonzalez, J. L., Ramirez, R., Hallen, J. M., & Guzman, R. A. (1997). Hydrogen-induced crack growth rate in steel plates exposed to sour environments. Corrosion, 53(12), p. 935-943.
18. Robertson, I. M. (2001). The effect of hydrogen on dislocation dynamics. Engineering fracture mechanics, 68(6), p.671-692.
19. Abdulkarim Omar Alfitouri , Mahmut Ahsen Savaş and Ali Evcil. Charpy Impact and Tension Tests of Two Pipeline Materials at Room and Cryogenic Temperatures. International Journal of Applied Engineering Research ISSN 0973-4562 Volume 13, Number 17 (2018) p.13321-13334
20. Godefroid, L. B., Cândido, L. C., Toffolo, R. V. B., & Barbosa, L. H. S. (2014).

Microstructure and mechanical properties of two API steels for iron ore pipelines. Materials Research, 17, p.114-120.

21. Jackson, T., Moses, J., & Stegmann, D. (2018, July). Sour Gas Plant Corrosion in the Presence of Elemental Sulfur. In *CORROSION 2018*. NACE International.
22. Fang, H. & Young, David & Nesic, Srdjan. (2008). Corrosion of mild steel in the presence of elemental sulfur. NACE - International Corrosion Conference Series.
23. Steudel, R. (1996). Mechanism for the formation of elemental sulfur from aqueous sulfide in chemical and microbiological desulfurization processes. *Industrial & Engineering Chemistry Research*, *35*(4), 1417-1423.
24. Maldonado-Zagal, S. B., & Boden, P. J. (1982). Hydrolysis of elemental sulphur in water and its effect on the corrosion of mild steel. *British Corrosion Journal*, *17*(3), 116-120.
25. MacDonald, D. D., Roberts, B., & Hyne, J. B. (1978). The corrosion of carbon steel by wet elemental sulphur. *Corrosion Science*, *18*(5), 411-425.
26. Schmitt, G. (1991). Effect of elemental sulfur on corrosion in sour gas systems. *Corrosion*, *47*(4), 285-308.
27. Radwan, A. B., Sliem, M. H., Okonkwo, P. C., Shibl, M. F., & Abdullah, A. M. (2017). Corrosion inhibition of API X120 steel in a highly aggressive medium using stearamidopropyl dimethylamine. Journal of Molecular Liquids, 236, 220-231.
28. Asmara, Y. P. (2018). The roles of H2S gas in behavior of carbon steel corrosion in oil and gas environment: a review. Jurnal Teknik Mesin Mercu Buana, 7(1), p. 37-43.

29. Panca Asmara, Y., & Che Ismail, M. (2009). A statistics approach for the prediction of CO2 corrosion in mixed acid gases. Corrosion and materials, 34(4), p. 25-30.
30. Asmara, Y. P., & Ismail, M. C. (2011). Study combinations effects of HAC in H2S/CO2 corrosion. *Journal of Applied Sciences*, *11*(10), p. 1821-1826.
31. Asmara, Y. P., & Ismail, M. C. (2012). Efficient design of response surface experiment for corrosion prediction in CO2 environments. Corrosion Engineering, Science and Technology, 47(1), p. 10-18.
32. Asmara, Y. P., Juliawati, A., & Sulaiman, A. (2013). Mechanistic model of stress corrosion cracking (scc) of carbon steel in acidic solution with the presence of H2s. In *IOP Conference Series: Materials Science and Engineering* (Vol. 50, No. 1, p. 012072).
33. Hua, Y., Barker, R., & Neville, A. (2015). The influence of SO2 on the tolerable water content to avoid pipeline corrosion during the transportation of supercritical CO2. *International Journal of Greenhouse Gas Control*, *37*, p. 412-423.
34. Nesic, S., & Vrhovac, M. (1999). A neural network model for CO2 corrosion of carbon steel. *JCSE: The Journal of Corrosion Science and Engineering*, *1*(April), p. 1-13.
35. Martin, C.F., Prediction CO2 Corrosion with the Presence of Low concentration Acetic Acid in Turbulent Flow Conditions, Master Thesis, UTP, 2009.
36. Lynch, S. P. (2007, January). Progress towards understanding mechanisms of hydrogen embrittlement and stress corrosion cracking. In *CORROSION 2007*. NACE International.
37. Birnbaum, H. K. (1987). On the mechanisms of hydrogen related fracture in

metals. *Environment Sensitive Fracture of Metals and Alloys, eds. Wei, RP, Duquette, DJ, Crooker, TW and Sedriks, AJ, Office of Naval Research, Arlington, VA*, 105-113.

38. Pfeil, L. B. (1926). The effect of occluded hydrogen on the tensile strength of iron. *Proceedings of the Royal Society of London. Series A, Containing Papers of a Mathematical and Physical Character*, *112*(760), 182-195.
39. Troiano, A. R. (2016). The role of hydrogen and other interstitials in the mechanical behavior of metals. *Metallography, Microstructure, and Analysis*, *5*(6), 557-569.
40. Oriani, R. A. (1972). A mechanistic theory of hydrogen embrittlement of steels. *Berichte der Bunsengesellschaft für physikalische Chemie*, *76*(8), 848-857.
41. Oriani, R. A. (1987). Whitney award lecture—1987: hydrogen—the versatile embrittler. *Corrosion*, *43*(7), 390-397.
42. Gerberich, W. W., & Chen, S. (1990). Environment-induced cracking of metals, fundamental processes: micromechanics. *Environment-Induced Cracking of Metals, eds. RP Gangloff, MB Ives (Houston, TX: NACE, 1990)*, 167.
43. Gerberich, W. W., Marsh, P., Hoehn, J., Venkataraman, S., & Huang, H. (1993). Hydrogen/plasticity interactions in stress corrosion cracking. *Corrosion–Deformation Interactions (CDI'92), Les Editions de Physique, Les Ulis*, 325-353.
44. Gerberich, W. W., Marsh, P. G., & Hoehn, J. W. (1996, January). Hydrogen induced cracking mechanisms-are there critical experiments?. In *Proceedings of the 1994 5th International Conference on the Effect of Hydrogen on the Behavior of Materials* (pp. 539-551). Minerals, Metals & Materials Soc (TMS).
45. Gangloff, R. P. (2003). *Hydrogen assisted cracking of high strength alloys*.

Aluminum Co of America Alcoa Center Pa Alcoa Technical Center.

46. Lynch, S. P. (2003). Mechanisms of hydrogen assisted cracking-a review. *Hydrogen effects on material behaviour and corrosion deformation interactions*, 449-466.